Comparison of $\delta^{18}O$ Analyses on Individual Planktic Foraminifer (*Orbulina universa*) Shells by SIMS and Gas-Source Mass Spectrometry

Jody B. Wycech[a,1], Daniel Clay Kelly[a], Reinhard Kozdon[b], Ian J. Orland[a], Howard J. Spero[c], John W. Valley[a]

[a]Department of Geoscience, University of Wisconsin-Madison, 1215 W. Dayton St., Madison, WI 53706, USA.

[b]Lamont-Doherty Earth Observatory of Columbia University, 61 Route 9W, Palisades, NY 10964, USA

[c]Department of Earth & Planetary Sciences, 1 Shields Ave, University of California Davis, Davis, CA 95616, USA

Corresponding author: Jody Wycech (jody.wycech@colorado.edu)

[1] Present Address: Cooperative Institute for Research in Environmental Science (CIRES), University of Colorado Boulder, Boulder, CO, USA.

Abstract

The oxygen isotope ($\delta^{18}O$) compositions of final chamber fragments of individual shells of the planktic foraminifer *Orbulina universa* were measured *in situ* via secondary ion mass spectrometry (SIMS) and by traditional gas-source mass spectrometry (GSMS) entailing acid digestion of sampled calcite. The paired SIMS-GSMS analyses were performed on final chamber fragments of fossil shells taken from the top of a sediment core (Holocene) as well as shells grown in laboratory culture. Multiple iterations of SIMS-GSMS analyses were conducted on final chamber fragments treated with a variety cleaning protocols. The series of paired analyses yielded an average SIMS-GSMS $\delta^{18}O$ offset ($\Delta^{18}O_{SIMS\text{-}GSMS}$) of -0.9 ± 0.1‰ (± 2 SE). The volume of material analyzed in 10-μm SIMS spots is ~10^5 times smaller than that analyzed by GSMS; hence, the extent to which these $\Delta^{18}O_{SIMS\text{-}GSMS}$ values represent real differences in analyte vs. instrumental factors remains unclear. Possible contributing factors to the SIMS-GSMS $\delta^{18}O$ difference include sample-standard mismatch by SIMS, differences in standardization of SIMS and GSMS, and non-calcite contaminants in samples. Although the two datasets are consistently offset, SIMS values reproduce inter-shell $\delta^{18}O$ variability delineated by shell fragment GSMS values. This strong positive covariance proved useful for bringing the two datasets into agreement (i.e. $\Delta^{18}O_{SIMS\text{-}GSMS} = 0$), and confirms that SIMS-based foraminifer $\delta^{18}O$ values record changes in calcification temperature and/or $\delta^{18}O$ of seawater. Whether shells of foraminifer taxa with differing microcrystalline structures, chemical composition, and/or preservation histories register a similar $\Delta^{18}O_{SIMS\text{-}GSMS}$ value is a subject of ongoing testing.

Keywords: oxygen isotopes; SIMS; isotope ratio mass spectrometry; planktic foraminifera

1 Introduction

Oxygen isotope ratios ($^{18}O/^{16}O$) measured from the biogenic calcite of microscopic shells grown by foraminifera, an extant group of marine protists with a rich fossil record, are one of the most widely used geochemical proxies for reconstructing past ocean-climate change (Pearson, 2012). However, reconstructions of ocean-climate history require the use of foraminifer shells that have retained their original oxygen isotope ($\delta^{18}O$) composition over time. Unfortunately, there is a paucity of pristinely preserved material in the deep-sea sedimentary archive as the chemistries of fossil foraminifer shells are often altered through isotopic exchange with sedimentary pore fluids (e.g. Killingley, 1983; Schrag et al., 1995; Pearson et al., 2001). To complicate matters, an added source of intra-shell $\delta^{18}O$ variability stems from the complex life histories and ecologies of planktic foraminifera. Such sources of intra-shell $\delta^{18}O$ heterogeneity are problematic for paleoclimate studies using conventional gas-source mass spectrometry (GSMS) because these analyses require acid digestion and isotope ratio measurements of whole shells that are often aggregate mixtures of carbonate that precipitated under differing environmental, ecological, and physiological conditions (e.g. Lohmann, 1995).

Over the past decade, the WiscSIMS laboratory has developed analytical techniques and procedures to address the aforementioned challenges to conventional GSMS $\delta^{18}O$ analyses. To this end, secondary ion mass spectrometry (SIMS) is now being used to make *in situ* $\delta^{18}O$ measurements on micrometer-scale domains within carbonate minerals, including individual foraminifer shells (Valley and Kita, 2009; Kozdon et al., 2009, 2011; Kita et al., 2009; Vetter et al., 2013). The ultra-high spatial resolution (~1-10 μm) of SIMS analyses permits isolated measurement of $\delta^{18}O$ in only the desired domain of an individual shell, and has been used to quantify the effects of diagenesis on the $\delta^{18}O$ of fossil planktic foraminifer shells (Kozdon et al.,

2013) and delineate intra-shell $\delta^{18}O$ signals that reflect experimentally induced geochemical bands in cultured planktic foraminifers (Vetter et al., 2013). SIMS has likewise been used to interrogate micrometer-scale $\delta^{18}O$ variability in carbonate materials as varied as corals (Rollion-Bard et al., 2007; Allison et al., 2010), nautiloids (Linzmeier et al., 2016), bivalves (Vihtakari et al., 2016), otoliths (Weidel et al., 2007; Hanson et al., 2010), and speleothems (Kolodny et al., 2003; Treble et al., 2007; Orland et al., 2009; Liu et al., 2015).

The aforementioned studies indicate that the use of SIMS to perform *in situ* $\delta^{18}O$ analyses on micrometer-scale domains within low-temperature carbonates represents a fundamental advance for enhancing the fidelity of paleoclimate reconstructions. Yet the potential of this technique cannot be fully realized without comparison to traditional whole-shell $\delta^{18}O$ values measured by GSMS. A tendency has emerged for SIMS measurements of $\delta^{18}O$ in low-temperature carbonates, at WiscSIMS and other labs, to be consistently lower than "paired" GSMS $\delta^{18}O$ values (Orland et al., 2015). Differences in GSMS and SIMS $\delta^{18}O$ data of typically 0-2‰ in biocarbonates and speleothems may arise from unrecognized analytical biases in the two techniques. The cause(s) of the previously observed SIMS-GSMS $\delta^{18}O$ difference ($\Delta^{18}O_{SIMS\text{-}GSMS}$) remains unclear and identifying the mechanism is beyond the scope of this study; nevertheless, few studies have directly compared SIMS and GSMS $\delta^{18}O$ measurements on the same material (Kozdon et al., 2011; Orland, 2012; Orland et al., 2015). Here, we conduct an inter-instrument $\delta^{18}O$ comparison by analyzing planktic foraminifer calcite using the extant, mixed-layer dwelling species *Orbulina universa*.

The species *O. universa* was selected for three reasons: (1) field and culturing studies have established the ecological affinities of this symbiont-bearing, mixed-layer species (e.g. Spero and Parker, 1985; Hemleben et al., 1989), (2) the relationship between $\delta^{18}O$ and temperature in *O.*

universa calcite has been empirically calibrated and shown to be very reproducible (e.g. Bemis et al., 1998), and (3) this species grows a large spherical chamber (Bé et al., 1973; Spero, 1988). The latter attribute is particularly advantageous because the final spherical chamber is massive (25-100 μg/shell), displays consistent geochemistry around its circumference (Fehrenbacher et al., 2015), and can be broken into chamber fragments for analysis without contamination from the juvenile chambers found in the earlier trochospiral part of the same shell. Thus, we measure $\Delta^{18}O_{SIMS\text{-}GSMS}$ values through analysis of identical foraminifer material using these two analytical techniques.

2 Materials and Methods

2.1 Core-Top Specimens

Shells of *O. universa* were handpicked from the uppermost 3 cm of piston core CH15-PC9-00 (PC9) taken atop Blake Ridge (2,790 m water depth; 31°55.691'N, 75°43.774'W) in the northwestern Atlantic (Fig. S1). Radiocarbon dating of this core-top sample has confirmed its Holocene age (Wycech et al., 2016). The sample was disaggregated in a pH-buffered solution (pH≈8) made of sodium hexametaphosphate, hydrogen peroxide (30 vol%), ammonium hydroxide, and distilled water, then rinsed with tap water over a 63-μm sieve. The resulting coarse fraction (>63 μm) was subsequently rinsed with distilled water before being oven-dried (30°C) overnight. The *O. universa* shells were handpicked from the >355 μm sieve-size fraction.

The presence of aragonitic pteropod shells and dissolution-prone species of planktic foraminifers (i.e. *Globigerinoides ruber,* Berger, 1968, 1970; Adelseck, 1978) possessing delicate spines indicates that the calcareous microfossil assemblage containing the *O. universa* shells experienced minimal carbonate dissolution. The surface textures of the *O. universa* shells were examined using back-scattered electron (BSE) imaging on a Hitachi S-3400N scanning

104 electron microscope (SEM) in variable pressure mode (Appendix B). The shells were not coated
105 for BSE imaging. Each whole shell was then manually broken into smaller fragments using a
106 surgical scalpel blade (e.g. Vetter et al., 2013). Whenever present, juvenile chambers were
107 removed with one or two of the final chamber fragments being used for *in situ* $\delta^{18}O$ analyses by
108 SIMS and the remaining fragments of the same final chamber being pooled for $\delta^{18}O$ analysis by
109 GSMS (Fig. 1). Sample weights of pooled chamber fragments used for the GSMS analyses
110 ranged from 10-90 μg. This "paired" approach allows us to make a direct comparison between
111 the SIMS and GSMS $\delta^{18}O$ values obtained from the spherical, final chambers of a population of
112 *O. universa* shells.

113 Three experiments were carried out to compare complementary SIMS and GSMS values for
114 the PC9 *O. universa* shells. Shell fragments analyzed by SIMS and GSMS in each experiment
115 were pre-treated in the same manner prior to final analytical preparation. In the first experiment,
116 spherical chambers were not processed beyond picking the shells from the sample, cracking them
117 open, and analyzing the calcite fragments. In the second experiment, the chamber fragments
118 were cleaned for 10 minutes in a 1:1 solution of 30% hydrogen peroxide and 0.1 N sodium
119 hydroxide at 65°C to remove organic matter. The cleaned fragments were then rinsed with
120 deionized water, sonicated for ~15 seconds in reagent grade methanol to remove material
121 adhering to the surface of the fragments, and rinsed two additional times in deionized water. The
122 third experiment entailed splitting the spherical chambers of each shell into three fragments; one
123 fragment was analyzed by GSMS without treatment, while a second and third fragment were
124 roasted *in vacuo* at 375°C for 30 minutes to remove labile organic carbon and water. The two
125 roasted fragments were subsequently used for analysis by GSMS and SIMS.

126 **2.2 Cultured Shells Grown under Controlled Conditions**

127 Paired SIMS-GSMS $\delta^{18}O$ analyses were also performed on eight *O. universa* shells grown in
128 the laboratory. These shells were cultured in 1995 as part of a larger experiment described by
129 Bemis et al. (1998) (Table S1). Specimens were maintained at constant temperature (22 ± 0.2°C),
130 $\delta^{18}O_{sw}$ = -0.25 ± 0.05‰ (VSMOW), salinity = 33.3‰, pH =8.04, and with an ambient [CO_3^{2-}]
131 (2250 μmol kg^{-1}). Many planktic foraminifer species, including *O. universa*, host algal symbionts
132 whose photosynthetic activity enhances biocalcification and increases intra-shell $\delta^{18}O$ variability
133 (Spero and Lea, 1993). The cultured specimens analyzed in this study were grown under varying
134 light conditions, which increases inter-shell $\delta^{18}O$ variability. Five of the specimens were grown
135 under a 12-hour light:12-hour dark cycle, two under low light intensity (26-30 μmol photons m^{-2}
136 s^{-1}) and three under high light intensity (400-700 μmol photons m^{-2} s^{-1}). An additional three
137 specimens were grown under continuous 24-hour low light intensity. The spherical chambers of
138 these cultured *O. universa* specimens calcified over a period of 3-9 days. The final spherical
139 chamber of each specimen was cracked into fragments as described in Section 2.1 and then
140 analyzed by GSMS and SIMS. The optical appearances and internal wall structures of the
141 cultured *O. universa* shells were similar to those of shells recovered from the PC9 core-top
142 (Appendix C).

143 **2.3 *In situ* $\delta^{18}O$ Measurement by SIMS**

144 The *O. universa* chamber fragments and three grains of the UWC-3 calcite standard ($\delta^{18}O$ = -
145 17.8‰ VPDB; Kozdon et al., 2009) were placed within a 10-mm-diameter circle, cast in a 25-
146 mm-diameter epoxy mount, ground to the level of best exposure in cross-section, polished with
147 carbonate-epoxy relief of less than ~1 μm (Kita et al., 2009), cleaned, and gold coated.
148 Secondary electron (SE) SEM images of each mounted shell fragment were taken in high-

149 vacuum mode to assess the quality of sample exposure and cross-section geometry prior to SIMS
150 analysis.

151 *In situ* $\delta^{18}O$ analyses were performed with a CAMECA IMS 1280 ion microprobe (SIMS) at
152 the WiscSIMS Laboratory, Department of Geoscience, University of Wisconsin-Madison using a
153 $^{133}Cs^{+}$ primary ion beam. Each series of 8-12 measurements of foraminifer calcite $\delta^{18}O$ was
154 bracketed by 4-6 consecutive $\delta^{18}O$ analyses (both before and after) of a UWC-3 standard grain in
155 the center of the sample mount. The 8 or more bracketing analyses were used to determine
156 calcite instrumental mass fractionation corrections and calculate the spot-to-spot reproducibility
157 (2 SD) for each set of foraminifer measurements. SIMS $\delta^{18}O$ values are reported in reference to
158 VPDB. After analysis, each SIMS pit was individually imaged (Appendix B) and examined by
159 SEM using the SE detector in high vacuum mode (see Section S1, Fig. S2). SIMS pits
160 intersecting cracks and/or epoxy were omitted from further interpretation. Raw and final
161 processed data are reported in Tables S2-S4.

162 For 10-μm SIMS spots (~1-μm deep) the primary ion beam intensity was ~1.2 nA,
163 comparable to Kozdon et al. (2013). The resulting secondary $^{18}O^{-}$, $^{16}O^{-}$, and $^{16}OH^{-}$ ions were
164 detected simultaneously from the 10-μm spots using three Faraday cup detectors with a typical
165 $^{16}O^{-}$ count rate of 2.3 x 10^{9} counts per second (cps). The energy bandpass width for secondary
166 ions was 40eV, which was re-centered during tuning for each analytical session. Simultaneous
167 measurement of $^{16}OH^{-}$ with $^{16}O^{-}$ and $^{18}O^{-}$ during SIMS analysis provides $^{16}OH^{-}/^{16}O^{-}$ ratios
168 (OH/O hereafter), which are used to gauge the relative hydrogen content in the sample, likely in
169 the form of water and/or organic matter. Even at ultra-high vacuum, the analytical chamber of
170 the SIMS contains detectable hydrous compounds, so the reported OH/O ratios were
171 background-corrected by subtracting the average OH/O of the UWC-3 (nominally anhydrous

metamorphic calcite) bracketing data from the OH/O ratio of the foraminifer. In addition to pit appearance, the OH/O ratio, $^{16}O^-$ count rate, and secondary ion yield (cps/nA) relative to the mean of the bracketing standard analyses served as a basis for assessing the quality of each intervening sample measurement (see Section S1). The total analytical time per spot was ~3 minutes for 10-µm spots including pre-sputtering. The average external precision (spot-to-spot reproducibility) for the 10-µm analyses, reported as two times the standard deviation of the bracketing standard measurements, was ±0.3‰ (±2 SD). A total of 160 SIMS measurements using 10-µm spots were performed on *O. universa* chamber fragments in addition to 93 bracketing measurements of the UWC-3 standard.

A second analytical setup with a primary-beam current of 19-21 pA and a spot size of ~3-µm (~1-µm deep) was used to investigate intra-chamber $\delta^{18}O$ variability (i.e. potential $\delta^{18}O$ variation during ontogenetic chamber thickening) and measure thin-walled *O. universa* shells from PC9 (e.g. Kozdon et al., 2009; Vetter et al., 2013). Secondary $^{18}O^-$, $^{16}O^-$, and $^{16}OH^-$ ions were detected simultaneously using an electron multiplier ($^{18}O^-$) and two Faraday cups ($^{16}O^-$, $^{16}OH^-$) with a mean $^{16}O^-$ count rate of 3.3 x 10^7 cps. The energy bandpass width for secondary ions was 40 eV for 3-µm $\delta^{18}O$ analyses, and was re-centered during tuning for each analytical session. The electron multiplier deadtime correction was 68 ns. In addition to pit appearance and OH/O, the $^{16}O^-$ count rate relative to the mean of the bracketing standard analyses served as a basis for assessing the quality of each $\delta^{18}O$ measurement (see Section S1). Prior to the November 2015 session, the electron multiplier gain was monitored before the third analysis of each group of UWC-3 standard analyses and, when necessary, the high voltage applied to the detector was increased by 1-6 volts to compensate for drift in the electron multiplier gain. A new, permanent protocol for gain adjustment was implemented during the November 2015 session, such that the

electron multiplier gain was monitored after each analysis and adjusted automatically as needed at a rate of 3-5 volts per hour. The total analytical time was ~7 minutes per 3-μm spot. The average precision (reproducibility on UWC-3) for the 3-μm analyses was ±0.7‰ (±2 SD, spot-to-spot). A total of 140 SIMS measurements using 3-μm spots were performed on *O. universa* chambers in addition to 93 bracketing measurements of the UWC-3 standard. The 3-μm analyses include the measurement of several spherical *O. universa* chambers from PC9 (untreated, n=6 shells) and culture (n=4 shells) that were also measured by 10-μm SIMS spots. Use of a smaller beam spot size (3-μm) made it possible to carry out SIMS $\delta^{18}O$ analyses on an additional 16 *O. universa* shells possessing thin-walled (<10 μm) chambers.

2.4 $\delta^{18}O$ Measurement by Gas Source Mass Spectrometry

Untreated and cleaned chamber fragments of *O. universa* shells from the PC9 core-top sample were analyzed at the University of California, Santa Cruz (UCSC) using a ThermoScientific Kiel IV carbonate device interfaced to a ThermoScientific MAT-253 dual-inlet isotope ratio mass spectrometer. The foraminifer fragments were digested in concentrated phosphoric acid (specific gravity=1.92 g/mL; Coplen et al., 1983) at 75°C. The external analytical precision is ±0.1‰ (2 SD) for the $\delta^{18}O$ measurement of fragmented foraminifer samples weighing 10-90 μg.

The $\delta^{18}O$ compositions of chamber fragments from cultured *O. universa* shells, as well as roasted chamber fragments of *O. universa* shells from the PC9 core-top, were measured at the University of California, Davis (UCD) using a Fisons Optima isotope ratio mass spectrometer fitted with a common acid bath auto-carbonate device. The foraminifer fragments were digested in concentrated phosphoric acid (specific gravity=1.92 g/mL; Coplen et al., 1983) at 90°C, and corrected for acid digestion fractionation by paired measurement with a Carrara marble standard

that was previously calibrated against NBS-19. External analytical precision is ±0.1‰ (2 SD) for $\delta^{18}O$ in the fragmented foraminifer samples weighing 10-90 μg. Foraminifer sample weights were comparable between the GSMS analyses completed in the UCSC and UCD laboratories.

For comparative purposes, three samples of the UWC-3 standard were analyzed by GSMS at both UCSC and UCD. For the analyses at UCSC, each sample weighed 70-90 μg and was composed of 2-5 calcite grains. At UCD, each sample was composed of a single grain that weighed 33-40 μg. The GSMS $\delta^{18}O$ values measured from the UWC-3 standard at UCSC and UCD were subsequently compared to those of UWC-3 previously measured by GSMS at the University of Wisconsin-Madison (Kozdon et al., 2009).

3 Results

3.1 Comparison of Paired SIMS-GSMS $\delta^{18}O$ Analyses

The $\delta^{18}O$ measurement of foraminifer calcite by SIMS is standardized to the GSMS-derived $\delta^{18}O$ value of the UWC-3 calcite standard. For this reason, we first analyzed the UWC-3 standard by GSMS in the same laboratories that measured the foraminifer fragments. GSMS $\delta^{18}O$ values (relative to VPDB) of UWC-3 analyzed by UCSC (-17.9 ± 0.2, 2SE) and UCD (-17.8 ± 0.1) are within analytical precision of the GSMS-derived published value (-17.8 ± 0.1‰, Kozdon et al., 2009) used for instrumental correction of the raw SIMS data (Table 1). We note that the GSMS measurements of UWC-3 carried out at UCSC and UCD were of a comparable size to fragmented foraminifer chambers (30-40 μg), and reproduced the established UWC-3 $\delta^{18}O$ value within 0.1‰.

The differing spatial resolutions (3 μm vs. 200 μm), weights (10^{-5} μg vs. 10 μg), and volumes (10 μm^3 vs. 10^7 μm^3) of material analyzed by SIMS and GSMS techniques necessitate thorough investigation of the intra-shell $\delta^{18}O$ variability captured by SIMS. To this end, $\delta^{18}O$ profiles were

generated across final chamber fragments using a series of 3-μm SIMS analyses (Fig. 2). The $\delta^{18}O$ values measured along each transect are within analytical uncertainty; hence, no consistent trends or patterns emerge from the series of 3-μm SIMS $\delta^{18}O$ measurements taken across the final chamber walls of the *O. universa* shells (n=15) collected from the PC9 core-top (Fig. 2). Consequently, the mean SIMS $\delta^{18}O$ value of each chamber was used for comparison to the paired GSMS $\delta^{18}O$ value.

The 3-μm and 10-μm SIMS analyses use different instrument settings with different levels of analytical precision. Thus, $\delta^{18}O$ measurements using both the 3-μm and 10-μm spots were conducted on the spherical chambers of several *O. universa* shells from the PC9 core-top (untreated, n=6 shells) and culture experiments (n=4 shells) (Fig. 3, Table 2). The 3-μm and 10-μm SIMS measurements from the same shells have comparable $^{16}O^-$ count rate ratios (foraminifer/bracketing standard = 0.92-1.03) and background-corrected OH/O ratios (0.006-0.010). Although the 3-μm analyses are less precise relative to the 10-μm analyses, the 3-μm and 10-μm $\delta^{18}O$ values measured from the same PC9 chambers are indistinguishable (unpaired t-test p-value of 0.928, Fig. 3A). Moreover, the 3-μm and 10-μm SIMS $\delta^{18}O$ data measured from all untreated shells taken from the PC9 core-top sample are statistically identical (unpaired t-test p-value of 0.52) (Fig. S3, Table S5). By contrast, the mean 3-μm $\delta^{18}O$ values for the cultured shells are, on average, 0.6 ± 0.6‰ (±2 SE) lower than those of mean 10-μm $\delta^{18}O$ values from the same shell (Fig. 3B). An unpaired t-test on the individual 10-μm and 3-μm SIMS $\delta^{18}O$ values indicates that the $\delta^{18}O$ difference measured among the cultured shells is statistically significant at the 95% confidence level. This difference between the SIMS $\delta^{18}O$ values acquired from 3-μm and 10-μm analysis pits in the cultured shells (Fig. 3B) led us to evaluate these two datasets separately in order to more thoroughly document possible inter-instrument differences.

264 We observe a consistent $\Delta^{18}O_{SIMS\text{-}GSMS}$ offset of -0.7 to -1.0‰ in all methodological
265 comparison experiments (Table 3). The $\Delta^{18}O_{SIMS\text{-}GSMS}$ values were calculated for each spherical
266 chamber to produce a dataset of per shell $\Delta^{18}O_{SIMS\text{-}GSMS}$ values that were averaged for each
267 experiment. The inter-instrument $\delta^{18}O$ differences are shown in Figure 4 where the paired SIMS-
268 GSMS values consistently fall below the theoretical 1-to-1 lines. The SIMS-GSMS $\delta^{18}O$
269 differences are not statistically different between experiments (Table 3), and the entire paired
270 dataset has an average $\Delta^{18}O_{SIMS\text{-}GSMS}$ value of -0.9 ± 0.1‰ (± 2 SE, n=66 pairs; Fig. 4F). A
271 salient aspect of the paired $\delta^{18}O$ data is the positive correlation between SIMS and GSMS values
272 over the ~3‰ range of $\delta^{18}O$ values measured from different *O. universa* spherical chambers (Fig.
273 4).

274 Although the $\Delta^{18}O_{SIMS\text{-}GSMS}$ values between experimental groups are similar, roasting and
275 cleaning by sonication and hydrogen peroxide may have a larger effect on $\delta^{18}O$ values measured
276 by one analytical technique. As a consequence, the effects of shell treatment on SIMS and
277 GSMS $\delta^{18}O$ values are investigated separately (see Section S2, Figs. S3-S4, Table S5).
278 Comparison of SIMS and GSMS $\delta^{18}O$ values of untreated and treated (cleaned, roasted) shells by
279 a t-test indicates that treatment does not have an appreciable effect on $\delta^{18}O$ values measured by
280 either analytical technique (Figs. S3-S4, Table S5 p-values). This inference is based on the
281 comparison of 'unpaired' values measured for the suite of shells in the untreated and roasted
282 experiments, which register a large degree of inter-shell $\delta^{18}O$ variability (~2-3‰) (Figs. S3-S4).
283 Paired GSMS $\delta^{18}O$ analyses of roasted and unroasted fragments of the same chamber remove
284 uncertainties related to inter-shell variability, and indicate that roasting decreases GSMS $\delta^{18}O$
285 values by 0.1‰ on average (Fig. 5, Table S7). The paired roasted-unroasted GSMS $\delta^{18}O$
286 difference is small, but statistically significant (paired t-test p-value=0.0015).

3.2 SIMS-GSMS $\delta^{18}O$ Differences

The positive correlation and strong covariance between the SIMS and GSMS $\delta^{18}O$ values raises the prospect that a simple correction or 'adjustment factor' may be appropriate for bringing the two datasets into agreement. Thus, the average $\Delta^{18}O_{SIMS\text{-}GSMS}$ value of 0.9‰ was added uniformly to the measured SIMS $\delta^{18}O$ values. We opted to adjust the SIMS values because GSMS has been the established technique for measuring isotope ratios in carbonates for nearly seven decades (e.g. McCrea, 1950; Epstein et al., 1953) and a majority of published data have been measured by GSMS. We note, however, that the offset between $\delta^{18}O_{GSMS}$ and $\delta^{18}O_{SIMS}$ values likely results from a complex combination of factors that affect the $\delta^{18}O$ values generated by the two techniques (see Section 4). The uniform adjustment made to the SIMS $\delta^{18}O$ values measured in the multiple experimental groups effectively removes the inter-instrument differences as reflected by the excellent agreement between the data and theoretical 1-to-1 lines (Fig. 6).

4 Discussion

Although the SIMS $\delta^{18}O$ values are offset from the paired GSMS values, the strong positive covariance between the two datasets over a 2-3‰ $\delta^{18}O$ range (Fig. 4) indicates that both analytical techniques record environmental changes that contributed to inter-shell $\delta^{18}O$ variation such as temperature, $\delta^{18}O_{sw}$ (Bemis et al., 1998) and physiological processes that affect microenvironment carbonate chemistry (Spero et al., 1997). Furthermore, the consistent ~0.9‰ $\Delta^{18}O_{SIMS\text{-}GSMS}$ value measured in each experiment allays concerns regarding sample treatment, and simplifies the proposed adjustment to SIMS $\delta^{18}O$ values measured from geologically young (Quaternary) *O. universa* shells. However, we caution that such an adjustment to SIMS $\delta^{18}O$ values acquired from shells belonging to foraminifer taxa possessing differing microcrystalline

structures, chemistries, and/or preservation histories, is a matter of ongoing testing. We also note that the adjustment herein proposed may not be appropriate for *in situ* $\delta^{18}O$ analyses carried out on foraminifer shells at other SIMS facilities since standards and operating conditions can vary.

4.1 SIMS-GSMS $\delta^{18}O$ Difference

The inter-instrument differences reported in this study may arise from both GSMS analyses entailing acid digestion of whole shells and *in situ* SIMS analyses that subsample micrometer-scaled domains within an individual shell. Differences in paired SIMS-GSMS $\delta^{18}O$ measurements of biogenic carbonates and speleothems have been previously reported, but the magnitude of the difference appears to vary with investigative procedures and the type of carbonate analyzed (Treble et al., 2007; Hanson et al., 2010; Allison et al., 2010; Orland, 2012; Liu et al., 2015; Orland et al., 2015). Such comparisons of SIMS and GSMS $\delta^{18}O$ values have revealed correlations to mineralogy (calcite, aragonite), sample age, and OH/O (Orland et al., 2015). Although existing empirical $\delta^{18}O$-temperature calibrations are based on GSMS measurements, neither SIMS nor GSMS $\delta^{18}O$ values should be regarded, *a priori*, as being more accurate. Furthermore, it is noted that SIMS analyses entail the isolated measurement of micrometer-scale targets, which permits the operator to avoid irregular or altered appearing domains. Thus, the mean SIMS $\delta^{18}O$ value of each chamber may be restricted to specific sub-domains of a test and not represent the bulk $\delta^{18}O$ composition of larger samples measured by GSMS.

4.2 GSMS Caveats

GSMS is the primary technique used for $\delta^{18}O$ measurement of foraminiferal calcite. In the past, problems with these conventional analyses were attributed to inter-lab calibration, gas leaks, incomplete acid digestion of the sample, surface area differences between the sample and

standard (*sensu* Wacker et al., 2013), analysis of water or organics (Oehlerich et al., 2013), or sample-reference gas misbalance (Potts, 1992; Wright, 1998). The two GSMS laboratories that analyzed *O. universa* chambers reproduced the $\delta^{18}O$ value of the UWC-3 calcite standard within 0.1‰ of the published value obtained at University of Wisconsin (Kozdon et al., 2009) even though the measurements were performed using different acid-digestion temperatures, sample sizes, and instrumental set-ups (Kiel device at 70ºC versus common acid bath at 90ºC). On the other hand, foraminifer sample treatment in this study does appear to have a minor effect on the $\delta^{18}O$ value measured by the acid-digestion technique given that *in vacuo* roasting of *O. universa* fragments decrease GSMS $\delta^{18}O$ values by 0.1‰ on average (Fig. 5, Table S7). Overall, the results of the UWC-3 analyses and the roasting experiment suggest that less than 30% of the measured 0.9‰ SIMS-GSMS $\delta^{18}O$ difference can be attributed to analytical aspects of the GSMS analyses. Below, we evaluate other explanations for the SIMS-GSMS $\delta^{18}O$ differences herein documented.

4.3 Potential causes of $\Delta^{18}O_{SIMS\text{-}GSMS}$

4.3.1 Matrix Effects

Stable isotope analysis by SIMS is a comparative technique and requires a reference material that matches the sample in mineralogy, chemical composition, and microcrystalline texture (Valley and Kia 2009, Sliwinski et al. 2016). The biogenic processes by which foraminifers precipitate their shells (e.g. de Nooijer et al., 2014) are fundamentally different from the recrystallization that occurs in a granulite facies marble that formed the UWC-3 standard. This is noteworthy because these abiotic/biotic processes give rise to carbonates with different microstructures, and the SIMS analyses performed in this study were standardized with the assumption that the instrumental mass fractionation (IMF) of the UWC-3 analyses matches that

of the samples. Such an assumption may be overly simplistic.

SIMS and GSMS analyses assume the analyzed foraminifers have calcite mineralogy. However, a small component (≤4.5%) of *O. universa* shells may be composed of the unstable calcium carbonate polymorph, vaterite (Jacob et al., 2017), which has a SIMS IMF and GSMS acid-fractionation factor that might differ from calcite (Kim and O'Neil 1997). Yet, preservation of foraminifer vaterite by SIMS and/or GSMS is an unlikely explanation for the $\Delta^{18}O_{SIMS\text{-}GSMS}$ values in this study due to the significant amount of time elapsed between calcification and analysis (i.e., 20 years for cultured shells, ~1,870 years for core-top shells).

The microcrystalline texture of foraminifer shells could also affect IMF thereby causing differences between SIMS $\delta^{18}O$ analyses of biogenic carbonate samples and a standard that crystallized at high temperatures. Such an issue is evidenced by previous SIMS analyses of nautiloid shells in which the measurements of more porous domains, imaged by SEM, correlated with $\delta^{18}O$ values that are ~0.8‰ lower (Linzmeier et al., 2016). Furthermore, foraminifer $\delta^{18}O$ values measured with SIMS may be affected by oxygen-bearing contaminant phases such as water or organics that have isotope ratios, IMF, and/or SIMS oxygen-ionization probabilities that differ from calcite. The OH/O ratios measured from *O. universa* chambers in this study indicate that the foraminifer matrix contains a hydrogen-bearing phase that was partly removed by vacuum roasting (Fig. 7).

Given our current understanding, a mismatch between the UWC-3 standard and the foraminifer matrix is likely a major source of the SIMS-GSMS $\delta^{18}O$ difference reported in all experimental iterations of this study. Unfortunately, identifying a homogeneous calcite standard that is perfectly matched to foraminifer shells for SIMS analysis is challenging due to the natural variability and complex mechanisms of biogenic calcification. With the possibility of a standard-

sample mismatch in mind, we consider other matrix-related factors such as differences in minor element composition, crystal size, the presence of water and organic matter, or high-$\delta^{18}O$ domains in foraminifers that are selectively avoided by SIMS. These effects are discussed below.

4.3.2 Cation composition and Matrix Effects

The importance of cation composition for correcting matrix effects on SIMS analyses in carbonates has long been known (Eiler et al., 1997, 2002; Valley and Kita, 2009), and it has recently been shown that minor Fe concentrations can have a large effect on carbonate IMF (Sliwiński et al., 2016, 2017). These studies indicate that minor- and possibly trace-element composition of calcite (i.e., Mg, Fe, Mn, Sr, Ba) need to be examined in more detail for their effect on carbonate IMF. We note that the UWC-3 calcite standard has higher concentrations of these elements than are published for *O. universa* (Table 4). Analysis of newly calibrated inorganic calcite standards indicates that the chemical compositions for *O. universa* in Table 4 cause systematic differences in IMF, and correcting for these differences would raise the sample $\delta^{18}O$ values reported here by 0.3-0.7‰ (Sliwinski et al. 2016, 2017; Sliwinski and Kitajima, pers. comm., Feb. 2018). Thus, IMF differences attributed to minor- and trace-element content of *O. universa* vs. UWC-3 may be a major cause of the $\Delta^{18}O_{SIMS\text{-}GSMS}$ values reported here, however a more detailed correction is beyond the scope of this paper because IMF values can change from session to session and thus calibration standards must be run at the same time as samples. At this time of this study, the new calcite standards had not been calibrated, and so neither the IMF of the new standards or the minor element compositions of *O. universa* were analyzed. Future studies will evaluate the importance of minor element substitutions for SIMS analysis of calcite in more detail.

401 **4.3.3 SIMS Measurement of Matrix-Bound Organics**

402 SIMS $\delta^{18}O$ analysis involves the measurement of all oxygen-bearing phases in the excavated
403 SIMS pit, which includes organic matter, water, and/or sulfate. These shell components are not
404 thought to contribute to the CO_2 analyzed by GSMS during phosphoric acid digestion. Thus,
405 SIMS measurement of biogenic carbonates will be affected if organics present in the volume of
406 the SIMS pit. Organic matter could form inclusions, be bound within the calcite matrix (Spero,
407 1988) or occur as nano-phases along grain boundaries (Cuif et al., 2012). Relatively young
408 (modern to Miocene-aged) foraminifer shells are composed of 0.02-0.2% organics, typically
409 amino acids and proteins that contain up to 25% oxygen (King and Hare, 1972; Robbins and
410 Brew, 1990).

411 The cleaning and sonication treatment was performed to remove shell organics in *O.*
412 *universa*, and the roasting experiment was performed to remove labile organic compounds and
413 associated hydrated phases, while leaving refractory compounds within the matrix. Organics in
414 biogenic carbonates are typically distributed throughout the mineral matrix in inter- and intra-
415 crystalline voids, and have proven difficult to remove even with extreme cleaning techniques
416 such as powdering and bleaching (Gaffey, 1990; Ren et al., 2009). The refractory nature of such
417 organics is evidenced by the retention of a primary $^{15}N/^{14}N$ geochemical signal in 212 Ma
418 Triassic corals (Frankowiak et al., 2016). These observations are further supported by the fact
419 that our hydrogen peroxide cleaning procedure had no discernible effect on either the SIMS or
420 GSMS $\delta^{18}O$ values (Figs. S3-S4, Tables 3, S5).

421 Direct comparison of GSMS $\delta^{18}O$ values measured from untreated and roasted fragments of
422 the same *O. universa* shell chamber yields an offset range of 0.1 to -0.2‰ (Table S7) with an
423 average decrease in $\delta^{18}O$ for roasted samples of 0.1 ± 0.1‰ (2 SD; Fig. 5). However, we note

424 that the fragments looked grey in color after roasting, evidence of organic carbon maturation.
425 This observation implies reaction, but ineffective removal of refractory organic contaminants.
426 Still, the roasted chambers (n=13) have lower OH/O ratios than the untreated, cleaned, and
427 cultured chambers, indicating that a portion of the water and/or volatile organic contaminants are
428 removed by roasting (Fig. 7). The lower GSMS $\delta^{18}O$ values registered by the roasted fragments
429 are consistent with data from previous experiments in which GSMS $\delta^{18}O$ values of crushed,
430 vacuum-roasted foraminifers are 0-0.5‰ lower than the $\delta^{18}O$ values of crushed unroasted
431 foraminifers (e.g. Emiliani, 1966; Erez and Honjo, 1981). These earlier studies compared only a
432 few roasted and unroasted samples that were comprised of hundreds of planktic foraminifer
433 shells. By contrast, the current dataset is the first to compare GSMS $\delta^{18}O$ values from roasted
434 and unroasted material from isotopically identical foraminifer shell fragments.

435 The effect of organic contamination on SIMS $\delta^{18}O$ values is difficult to evaluate with the
436 data at hand and, unfortunately, the effect of roasting on SIMS $\delta^{18}O$ values remains unknown as
437 *in situ* measurements were not performed on unroasted and roasted fragments of the same
438 chambers. Oxygen composes a minor portion of amino acids and proteins that are present within
439 the foraminifer calcite at low concentrations (King and Hare, 1972; Robbins and Brew, 1990),
440 but the relative sensitivity factors and instrument bias are not known for the conditions of our
441 SIMS analyses. Nevertheless, the consistent $\Delta^{18}O_{SIMS\text{-}GSMS}$ values for all experiments (Fig. 4)
442 suggest that measurement of refractory organics in the foraminifer calcite by SIMS – and not
443 GSMS – may be a contributing factor to the inter-instrument difference.

444 **4.3.4 SIMS Measurement of Matrix-Bound Sulfate**

445 Another secondary, oxygen-bearing phase that may be measured by SIMS but not GSMS is
446 carbonate-associated sulfate (CAS). In *O. universa* calcite, CAS concentration ranges from

1,000-1,800 ppm and tracks the $[SO_4^{2-}]/[Ca^{2+}]$ ratio of seawater (Paris et al., 2014). In order to evaluate whether CAS contributes to the observed $\Delta^{18}O_{SIMS\text{-}GSMS}$, we reference analysis of a calcite speleothem, where CAS concentrations are known to track atmospheric SO_2 sourced by volcanogenic and anthropogenic emissions (e.g. Frisia et al., 2008; Wynn et al., 2010; Borsato et al., 2015). Consequently, CAS concentrations in speleothem calcite have increased by a factor of 10 (from <10 ppm to ~100 ppm) during the past ~150 years due to fossil fuel emissions (Frisia et al., 2008; Wynn et al., 2010; Borsato et al., 2015). Yet, $\Delta^{18}O_{SIMS\text{-}GSMS}$ values measured in a speleothem that grew continuously from pre-industrial to modern are temporally invariant within SIMS analytical precision (±0.5‰, 2SD; Orland, 2012). The observation that speleothem $\Delta^{18}O_{SIMS\text{-}GSMS}$ values do not measurably scale with CAS concentration suggests that low amounts of CAS (10-100 ppm) do not contribute to the $\delta^{18}O$ offset. However, SIMS analysis of the relatively high CAS concentration (~1000 ppm) in foraminifers is still a possible explanation for the $\Delta^{18}O_{SIMS\text{-}GSMS}$ values reported herein for *O. universa* calcite.

4.3.5 SIMS Measurement of Matrix-Bound Water

Biogenic carbonates contain water within the organic or carbonate matrix, on grain boundaries, in fluid inclusions, and/or chemically bound to the matrix as OH^- ions (Gaffey, 1988). Thus, another contribution to the SIMS-GSMS $\delta^{18}O$ difference may be from other contaminants in the foraminifer matrix, such as water or hydroxyl ions. An important result of this study is that the roasted chambers (n=13) have lower OH/O ratios than the untreated, cleaned, and cultured chambers, but still have a comparable SIMS-GSMS $\delta^{18}O$ offset (Fig. 7). SIMS analyses on basaltic glass at the University of Wisconsin-Madison indicate that 1 wt% water increases OH/O ratios by approximately 0.002. The relative sensitivity factors for glass and carbonate will differ, but this comparison provides an approximate value for the weight

470 percent of water. Assuming the relative sensitivity factors are equal, the untreated, cleaned, and
471 cultured shells (~0.011) have water contents that are consistent with those (~3 wt%) previously
472 reported for skeletal carbonates (Hudson, 1967; Gaffey, 1988, 1990). The removal of unbonded
473 water in the foraminifer shell, rather than removal of OH or organics or a change in shell matrix,
474 during roasting is the most likely explanation for the lower OH/O ratios of our roasted shell
475 fragments (Fig. 7). Results from a prior study show that samples roasted *in vacuo* at temperatures
476 (150°C for 8 hours and 105 °C for 24 hours) lower than those used in this study have a reduced
477 H_2O and OH absorption signal in the reflected 0.5-2.5 μm wavelength spectra (Gaffey et al.,
478 1991). The comparable $\Delta^{18}O_{SIMS\text{-}GSMS}$ values registered by the untreated, cleaned, and roasted
479 chambers suggest that the H-bearing phase, most likely unbonded water, lost during roasting is
480 not a major factor in the SIMS-GSMS $\delta^{18}O$ difference. Although unroasted foraminifers are
481 exposed to high vacuum prior to and during SIMS analysis, we cannot rule out SIMS
482 measurement of chemically bound water in foraminifer calcite.

483 **4.3.6 Measurement of Secondary Calcite Phases**

484 Field studies have shown that many mixed-layer dwelling species sink into deeper, cooler
485 waters during reproduction (gametogenesis) at the end of their life cycles where an ^{18}O-enriched
486 crust is rapidly added to the outer surface of a shell (e.g. Bé, 1980; Duplessy et al., 1981;
487 Lohmann, 1995; Kozdon et al., 2009). Approximately 4 μg of gametogenic (GAM) calcite is
488 added to the outer surface of *O. universa* shells during the final 24 hours of calcification
489 (Hamilton et al., 2008) near the deep chlorophyll maximum as the species transitions from its
490 normal life through meiosis and gamete production (Bé, 1980). In addition, diagenesis can add
491 sub-micrometer to micrometer scale carbonate phases onto foraminifer shells at relatively cold
492 bottom-water temperatures, which would then bias whole-shell GSMS measurements of planktic

493 foraminifers toward higher-$\delta^{18}O$ values (Killingley, 1983; Pearson et al., 2001, 2007; Sexton et
494 al., 2006; Kozdon et al., 2013; Edgar et al., 2015). Unfortunately, measuring the $\delta^{18}O$ of such
495 minute (<3 μm) early diagenetic crystallites (e.g. Groeneveld et al., 2008) and thin GAM crusts
496 (~2 μm) on *O. universa* with SIMS is precluded by their proximity to the epoxy mounting
497 medium. Moreover, the secondary calcite phases cannot be removed or separated prior to GSMS
498 analysis and would, in theory, contribute to the SIMS-GSMS $\delta^{18}O$ difference.

499 The *O. universa* shells recovered from the core-top sample exhibit variable surface structures
500 and optical appearances, which may be attributed to diagenetic alteration or the addition of GAM
501 calcite (Fig. S5A-E). However, the $\Delta^{18}O_{SIMS\text{-}GSMS}$ values are not dependent upon *O. universa*
502 shell surface textures or optical appearances (Fig. S5F-G), which suggests that the SIMS-GSMS
503 differences are not related to inter-shell differences in preservation or gametogenesis. Moreover,
504 the cultured *O. universa* chambers analyzed in this study were never exposed to water column or
505 seafloor conditions, yet they still yield an average $\Delta^{18}O_{SIMS\text{-}GSMS}$ value of -0.7 ± 0.1‰. This
506 result suggests that the selective analysis of diagenetic or GAM crust by only GSMS is an
507 unlikely cause of the inter-instrument $\delta^{18}O$ difference.

508 **5 Conclusions**

509 Paired $\delta^{18}O$ measurements were performed on the final (spherical) chamber of the same *O.*
510 *universa* shell using *in situ* SIMS and acid-digestion GSMS analyses, permitting the direct
511 comparison of the two analytical techniques. Analysis of individual foraminifer chambers was
512 carried out on specimens grown in laboratory culture and fossil (Holocene) shells collected from
513 the upper 3 cm of a sediment core. Comparison of the two datasets yields an average $\Delta^{18}O_{SIMS\text{-}GSMS}$ value of -0.9 ± 0.1‰ – an inter-instrumental offset that equates to a ~4°C difference in
515 reconstructed temperatures (Mulitza et al., 2003). Treatment of the core-top shells did not

516 remove the inter-instrument difference given that the $\Delta^{18}O_{SIMS\text{-}GSMS}$ values are statistically
517 indistinguishable between experiments. Strong positive covariance between the inter-shell SIMS
518 and GSMS $\delta^{18}O$ values indicates that secular variation expressed in foraminifer $\delta^{18}O$
519 stratigraphies compiled via conventional GSMS analyses is captured by SIMS analyses of age-
520 equivalent foraminifers.

521 The inter-instrument $\delta^{18}O$ differences measured in this study likely stem from a combination
522 of such factors as SIMS measurement of oxygen in chemically-bound water and refractory
523 organic matter, sample treatment and conditions during GSMS analysis, differences in minor
524 element concentration of samples vs. standards, and/or a change in the SIMS oxygen isotope
525 instrumental mass fractionation due to the differing crystalline microstructures of the foraminifer
526 shells in comparison to the coarse single crystals of the UWC-3 calcite standard. Determining the
527 roles of these various mechanisms in causing the inter-instrument differences herein reported is
528 beyond the scope of the present study and will require further testing. Furthermore, we caution
529 that the 0-2‰ SIMS-GSMS differences measured for carbonates in this and other studies
530 (Orland et al., 2015) may not exist for $\delta^{18}O$ analyses performed on foraminifer taxa with
531 significantly different shell microstructures, porosities, and/or burial histories. This is especially
532 true for foraminifer shells recovered from older, more deeply buried sediments that have
533 experienced a greater degree of degradation of organic compounds (Gaffey, 1990) and release
534 water bound within the shell matrix (Gaffey, 1985). Thus, this study motivates future research to
535 investigate the causes of these differences.

536 **Acknowledgments**

537 Funding was provided by the National Science Foundation (grant number OCE-1405224,
538 D.C.K. and R.K.; OCE-0550703, H.S.; AGS-1603065, I.J.O.), Shell Oil Company (D.C.K.), and

539 the U.S. Department of Energy, Office of Basic Energy Sciences, Geosciences Division (award
540 number DE-FG02-93ER14389, J.W.V.). WiscSIMS is supported by NSF (EAR-1355590) and
541 UW-Madison. Shipboard coring operations supported by the United States Geological Survey
542 (William Dillon) and Woods Hole Oceanographic Institute (D.C.K., Richard Norris). The crew
543 of the RV Cape Hatteras, Charles Paull, and William Ussler conducted coring operations. We
544 thank Ellen Roosen (WHOI Core Repository) for core sampling assistance. Cultured shells were
545 grown by C. Hamilton (UC Davis). Conventional stable isotope measurements were assisted by
546 Dyke Andreason (UC Santa Cruz) and Edward Chu (UC Davis). Brian Hess prepared epoxy
547 mounts. Kouki Kitajima and Noriko Kita assisted SIMS measurements. We thank Adam Denny,
548 Benjamin Linzmeier, Maciej Śliwiński, and Nick Levitt for fruitful discussions. We also thank
549 one anonymous reviewer and Kevin McKeegan for their suggestions that helped improve the
550 manuscript.

551 **References**

552 Adelseck Jr., C.G., 1978. Dissolution of deep-sea carbonate: preliminary calibration of
553 preservational and morphologic aspects. Deep-Sea Res. II. 25, 1167–1185.

554 Allison N., Finch A.A. and EIMF, 2010. The potential origins and palaeoenvironmental
555 implications of high temporal resolution $\delta^{18}O$ heterogeneity in coral skeletons. Geochim.
556 Cosmochim. Ac. 74, 5537–5548.

557 Bemis B.E., Spero H. J., Bijma J. and Lea D.W., 1998. Reevaluation of the oxygen isotopic
558 composition of planktonic foraminifera: Experimental results and revised paleotemperature
559 equations. Paleoceanography. 13, 150–160.

560 Bender M.L., Lorens R.B. and Williams D.F., 1975. Sodium, Magnesium and Strontium in the
561 Tests of Planktonic Foraminifera. Micropaleontology. 21, 448–459.

562 Berger W.H., 1968. Planktonic foraminifera: selective solution and paleoclimatic interpretation.
563 Deep-Sea Res. II. 15, 31–43.

564 Berger W.H., 1970. Planktonic Foraminifera: Selective Solution and the Lysocline. Mar. Geol. 8,
565 111–138.

566 Bé A.W., Harrison S. and Lott L., 1973. *Orbulina universa* d'Orbigny in the Indian Ocean.
567 Micropaleontology 19, 150–192.

568 Bé A.W., 1980. Gametogenic calcification in a spinose planktonic foraminifer, *Globigerinoides*
569 *sacculifer* (Brady). Mar. Micropaleontol. 5, 283–310.

570 Borsato A., Frisia S., Wynn P.M., Fairchild I.J. and Miorandi R., 2015. Sulphate concentration in
571 cave dripwater and speleothems: long-term trends and overview of its significance as proxy
572 for environmental processes and climate changes. Quaternary Sci. Rev. 127, 1–13.

573 Boyle E.A., 1981. Cadmium, zinc, copper, and barium in foraminifera tests. Earth Planet. Sc.
574 Lett. 53, 11–35.

575 Carpenter S. and Lohmann K.C., 1992. Sr /Mg ratios of modern marine calcite: Empirical
576 indicators of ocean chemistry and precipitation rate. Geochim. Cosmochim. Ac. 56, 1837–
577 1849.

578 Coplen, T.B., Kendall, C., Hopple, J., 1983. Comparison of stable isotope reference samples.
579 Nature. 302, 236–238.

580 Cuif J.P., Dauphin Y., Nehrke G., Nouet J. and Perez-Huerta A., 2012. Layered Growth and
581 Crystallization in Calcareous Biominerals: Impact of Structural and Chemical Evidence on
582 Two Major Concepts in Invertebrate Biomineralization Studies. Minerals. 2, 11–39.

583 de Nooijer L.J., Spero H.J., Erez J., Bijma J. and Reichart G.J., 2014. Biomineralization in
584 perforate foraminifera. Earth Sci. Rev. 135, 48–58.

585 Delaney M.L., Bé A.W. and Boyle E.A., 1985. Li, Sr, Mg, and Na in foraminiferal calcite shells
586 from laboratory culture, sediment traps, and sediment cores. Geochim. Cosmochim. Ac. 49,
587 1327–1341.

588 Duplessy J.C., Blanc P.L. and Bé A.W., 1981. Oxygen-18 Enrichment of Planktonic
589 Foraminifera due to Gametogenic Calcification below the Euphotic Zone. Science. 213,
590 1247–1250.

591 Edgar K.M., Anagnostou E., Pearson P.N. and Foster G.L., 2015. Assessing the impact of
592 diagenesis on $\delta^{11}B$, $\delta^{13}C$, $\delta^{18}O$, Sr/Ca and B/Ca values in fossil planktic foraminiferal calcite.
593 Geochim. Cosmochim. Ac. 166, 189–209.

594 Eggins S., Sadekov A. and DeDeckker P., 2004. Modulation and daily banding of Mg/Ca in tests
595 by symbiont photosynthesis and respiration: a complication for seawater thermometry? Earth
596 Planet. Sc. Lett. 225, 411–419.

597 Eiler J.M., Valley J.W. and Graham C.M., 1997. Standardization of SIMS Analysis of O and C
598 isotope ratios in Carbonates from ALH-84001. Lunar Planet. Sci. XXVIII. Lunar Planet.
599 Inst., Houston. #327(abstr.).

600 Eiler J.M., Valley J.W., Graham C.M. and Fournelle J. H., 2002. Two populations of carbonate
601 in ALH84001: Geochemical evidence for discrimination and genesis. Geochim. Cosmochim.
602 Ac. 66, 1285–1303.

603 Emiliani C., 1966. Paleotemperature Analysis of Caribbean Cores P6304-8 and P6304-9 and a
604 Generalized Temperature Curve for the past 425,000 Years. Geology. 74, 109–124.

605 Epstein S., Buchsbaum R., Lowenstam H.A. and Urey H.C., 1953. Revised carbonate-water
606 isotopic temperature scale. Bull. Geol. Soc. Am. 64, 1315–1326.

607 Erez J. and Honjo S., 1981. Comparison of isotopic composition of planktonic foraminifer in
608 plankton tows, sediment traps, and sediments. Palaeogeogr. Palaeocl. 33, 129–156.

609 Fehrenbacher J.S., Spero H.J., Russell A.D., Vetter L. and Eggins S., 2015. Optimizing LA-ICP-
610 MS analytical procedures for elemental depth profiling of foraminifera shells. Chem. Geol.
611 407-408, 2–9.

612 Frankowiak K., Wang X.T., Sigman D.M., Gothmann A.M., Kitahara M.V., Mazur M., Meibom
613 A. and Stolarski J., 2016. Photosymbiosis and the expansion of shallow-water corals. Sci.
614 Adv. 2, 1–7.

615 Frisia S., Borsato A. and Susini J., 2008. Synchrotron radiation applications to past volcanism
616 archived in speleothems: An overview. J. Volcanol. Geoth. Res. 177, 96–100.

617 Gaffey S., 1985. Reflectance spectroscopy in the visible and near-infrared (0.35-2.55 μm):
618 Applications in carbonate petrology. Geology. 13, 270–273.

619 Gaffey S. J., 1988. Water in skeletal carbonates. J. Sediment. Petrol. 58, 397–414.

620 Gaffey S., 1990. Skeletal Versus Nonbiogenic Carbonates UV-Visible-Near IR (0.3-2.7 μm)
621 Reflectance Properties. In Spectroscopic Characterization of Minerals and Their Surfaces
622 (eds. L. M. Coyne, S. W. McKeever, and E. S. Blake). Am. Chem. Soc., Washington, D.C.
623 415, pp. 94–116.

624 Gaffey S., Kolak J. and Bronnimann C.E., 1991 Effects of drying, heating, annealing, and
625 roasting on carbonate skeletal material, with geochemical and diagenetic implications.
626 Geochim. Cosmochim. Ac. 55, 1627–1640.

627 Groeneveld J., Nurnberg D., Tiedemann R., Reichart G.J., Steph S., Reuning L., Crudeli D. and
628 Mason P., 2008. Foraminiferal Mg/Ca increase in the Caribbean during the Pliocene:
629 Western Atlantic Warm Pool formation, salinity influence, or diagenetic overprint?
630 Geochem. Geophy. Geosy. 9, 1–21.

631 Hamilton C.P., Spero H.J., Bijma J. and Lea D.W., 2008. Geochemical investigation of
632 gametogenic calcite addition in the planktonic foraminifera *Orbulina universa*. Mar.
633 Micropaleontol. 68, 256–267.

634 Hanson N.N., Wurster C.M., EIMF and Todd C.D., 2010. Comparison of secondary ion mass
635 spectrometry and micromilling/continuous flow isotope ratio mass spectrometry techniques
636 used to acquire intra-otolith $\delta^{18}O$ values of wild Atlantic salmon (Salmo salar). Rapid
637 Commun. Mass Spectrom. 24, 2491–2498.

638 Hemleben C., Spindler M. and Anderson O., 1989. Modern Planktonic Foraminifera, Springer-
639 Verlag, New York.

640 Hudson J.D., 1967. The elemental composition of the organic fraction, and the water content, of
641 some recent and fossil mollusc shells. Geochim. Cosmochim. Ac. 31, 2361–2378.

642 Jacob, D.E., Wirth, R., Agbaje, O.B.A., Branson, O., Eggins, S.M., 2017. Planktic foraminifera
643 form their shells via metastable carbonate phases. Nat. Commun. 8, 1–9.

644 Killingley J.S., 1983. Effects of diagenetic recrystallization on $^{18}O/^{16}O$ values of deep-sea
645 sediments. Nature. 301, 594–597.

646 Kim, S.T., O'Neil, J.R., 1997. Equilibrium and nonequilibrium oxygen isotope effects in
647 synthetic carbonates. Geochim. Cosmochim. Ac. 61, 3461–3475.

648 King K. Jr and Hare P.E., 1972. Amino Acid Composition of Planktonic Foraminifera: A
649 Paleobiochemical Approach to Evolution. Science. 175, 1461–1463.

650 Kita N.T., Ushikubo T., Fu B. and Valley J.W., 2009. High precision SIMS oxygen isotope
651 analysis and the effect of sample topography. Chem. Geol. 264, 43–57.

652 Kolodny Y., Bar-Matthews M., Ayalon A. and McKeegan K.D., 2003. A high spatial resolution
653 $\delta^{18}O$ profile of a speleothem using an ion-microprobe. Chem. Geol. 197, 21–28.

654 Kozdon R., Ushikubo T., Kita N.T., Spicuzza M.J. and Valley J.W., 2009. Intratest oxygen

isotope variability in the planktonic foraminifer *N. pachyderma*: Real vs. apparent vital effects by ion microprobe. Chem. Geol. 258, 327–337.

Kozdon R., Kelly D.C., Kita N.T., Fournelle J.H. and Valley J.W., 2011. Planktonic foraminiferal oxygen isotope analysis by ion microprobe technique suggests warm tropical sea surface temperatures during the Early Paleogene. Paleoceanography. 26, 1-17.

Kozdon R., Kelly D.C., Kitajima K., Strickland A., Fournelle J.H. and Valley J.W., 2013. *In situ* $\delta^{18}O$ and Mg/Ca analyses of diagenetic and planktic foraminiferal calcite preserved in a deep-sea record of the Paleocene-Eocene thermal maximum. Paleoceanography. 28, 517–528.

Lea D. W. and Boyle E.A., 1991. Barium in planktonic foraminifera. Geochim. Cosmochim. Ac. 55, 3321–3331.

Lea D. W., Mashiotta T.A. and Spero H. J., 1999. Controls on magnesium and strontium uptake in planktonic foraminifera determined by live culturing. Geochim. Cosmochim. Ac. 63, 2369–2379.

Linzmeier B.J., Kozdon R., Peters S.E. and Valley J.W., 2016. Oxygen Isotope Variability within Nautilus Shell Growth Bands ed. S. Kiel. PLOS ONE 11, 1-31.

Liu Y., GuoQiang T., XiaoXiao L., ChaoYong H. and XianHua L., 2015. Speleothem annual layers revealed by seasonal SIMS $\delta^{18}O$ measurements. Sci. China Earth Sci. 58, 1741–1747.

Lohmann G.P., 1995. A model for variation in the chemistry of planktonic foraminifera due to secondary calcification and selective dissolution. Paleoceanography. 10, 445–457.

McCrea J.M., 1950. On the Isotopic Chemistry of Carbonates and a Paleotemperature Scale. The J. Chem. Phys. 18, 849.

Mulitza S., Boltovskoy D., Donner B., Meggers H., Paul A. and Wefer G., 2003. Temperature: $\delta^{18}O$ relationships of planktonic foraminifera collected from surface waters. Palaeogeogr. Palaeocl. 202, 143–152.

Oehlerich M., Baumer M., Lücke A. and Mayr C., 2013. Effects of organic matter on carbonate stable isotope ratios ($\delta^{13}C$, $\delta^{18}O$ values) - implications for analyses of bulk sediments. Rapid Commun. Mass Spectrom. 27, 707–712.

Orland I.J., Bar-Matthews M., Kita N.T., Ayalon A., Matthews A. and Valley J.W., 2009. Climate deterioration in the Eastern Mediterranean as revealed by ion microprobe analysis of a speleothem that grew from 2.2 to 0.9 ka in Soreq Cave, Israel. Quaternary Res. 71, 27–35.

Orland I., 2012. Seasonality from speleothems: High-resolution ion microprobe studies at Soreq Cave, Israel. Ph.D. Thesis, University of Wisconsin-Madison.

Orland I., Kozdon R., Linzmeier B.J., Wycech J., Sliwiński M. G., Kitajima K., Kita N.T. and Valley J.W., 2015. Enhancing the Accuracy of Carbonate $\delta^{18}O$ and $\delta^{13}C$ Measurements by

690 SIMS. American Geophysics Union Conference. Am. Geophys. Union, San Francisco.
691 #PP52B-03(abstr.).

692 Paris G., Fehrenbacher J.S., Sessions A.L., Spero H.J. and Adkins J.F., 2014. Experimental
693 determination of carbonate-associated sulfate $\delta^{34}S$ in planktonic foraminifera shells.
694 Geochem. Geophy. Geosy. 15, 1452–1461.

695 Pearson P.N., Ditcheld P.W., Singano J., Harcourt-Brown K.G., Nicholas C.J., Shackleton N.J.
696 and Hall M.A., 2001. Warm tropical sea surface temperatures in the Late Cretaceous and
697 Eocene epochs. Nature. 415, 481–487.

698 Pearson P.N., Van Dongen B.E., Nicholas C.J., Pancost R.D., Schouten S., Singano J.M. and
699 Wade B.S., 2007. Stable warm tropical climate through the Eocene Epoch. Geology. 35,
700 211–214.

701 Pearson P.N., 2012. Oxygen isotopes in foraminifera: Overview and historical review. Paleontol.
702 Soc. Pap. 18, 1–38.

703 Potts P.J., 1992. Gas source mass spectrometry. In A Handbook of Silicate Rock Analysis
704 Springer US. pp. 546–565.

705 Ren H., Sigman D.M., Meckler A.N., Plessen B., Robinson R.S., Rosenthal Y. and Haug G.H.,
706 2009. Foraminiferal Isotope Evidence of Reduced Nitrogen Fixation in the Ice Age Atlantic
707 Ocean. Science. 323, 244–248.

708 Robbins L.L. and Brew K., 1990. Proteins from the organic matrix of core-top and fossil
709 planktonic foraminifera. Geochim. Cosmochim. Ac. 54, 2285–2292.

710 Rollion-Bard C., Mangin D. and Champenois M., 2007. Development and Application of
711 Oxygen and Carbon Isotopic Measurements of Biogenic Carbonate by Ion Microprobe.
712 Geostand. Geoanal. Res. 31, 39–50.

713 Rosenthal Y., Lohmann G.P., Lohmann K.C. and Sherrell R.M., 2000. Incorporation and
714 preservation of Mg in *Globigerinoides sacculifer*: Implications for reconstructing the
715 temperature and $^{18}O/^{16}O$ of seawater. Paleoceanography. 15, 135–145.

716 Russell A.D., Honisch B., Spero H.J. and Lea D.W., 2004. Effects of seawater carbonate ion
717 concentration and temperature on shell U, Mg, and Sr in cultured planktonic foraminifera.
718 Geochim. Cosmochim. Ac. 68, 4347–4361.

719 Sadekov A.Y., Eggins S.M. and De Deckker P., 2005. Characterization of Mg/Ca distributions in
720 planktonic foraminifera species by electron microprobe mapping. Geochem. Geophy. Geosy.
721 6, 1-14.

722 Schrag D.P., DePaolo D.J. and Richter F.M., 1995. Reconstructing past sea surface temperatures:
723 Correcting for diagenesis of bulk marine carbonate. Geochim. Cosmochim. Ac. 59, 2265–
724 2278.

725 Sexton P.F., Wilson P.A. and Pearson P.N., 2006. Microstructural and geochemical perspectives
726 on planktic foraminiferal preservation: “Glassy” versus ‘Frosty’. Geochem. Geophy. Geosy.
727 7, 1–29.

728 Śliwiński M.G., Kitajima K., Kozdon R., Spicuzza M.J., Fournelle J.H., Denny A. and Valley
729 J.W., 2016. Secondary Ion Mass Spectrometry Bias on Isotope Ratios in Dolomite-Ankerite,
730 Part I: $\delta^{18}O$ Matrix Effects. Geostand. Geoanal. Res. 40, 157–172.

731 Śliwiński M., Kitajima K., Spicuzza M.J., Orland I.J., Ishida A., Fournelle J.H. and Valley J.,
732 2017. SIMS bias on isotope ratios in Ca-Mg-Fe carbonates (Part III): $\delta^{18}O$ and $\delta^{13}C$ matrix
733 effects along the magnesite-siderite solid-solution series. Geostand. Geoanal. Res. 41. doi:
734 10.1111/ggr.12194.

735 Spero H. and Parker S.L., 1985. Photosynthesis in the symbiotic planktonic foraminifer *Orbulina*
736 *universa*, and its potential contribution to oceanic primary productivity. J. Foramin. Res. 15,
737 273–281.

738 Spero H., 1988. Ultrastructural examination of chamber morphogenesis and biomineralization in
739 the planktonic foraminifer *Orbulina universa*. Mar. Biol. 99, 9–20.

740 Spero H. and Lea D.W., 1993. Intraspecific stable isotope variability in the planktic foraminifera
741 *Globigerinoides sacculifer*: Results from laboratory experiments. Mar. Micropaleontol. 22,
742 221–234.

743 Spero H., Bijma J., Lea D.W. and Bemis B.E., 1997. Effect of seawater carbonate concentration
744 on foraminiferal carbon and oxygen isotopes. Nature. 390, 497–500.

745 Towe K.M. and Cifelli R., 1967. Wall Ultrastructure in the Calcareous Foraminifera:
746 Crystallographic Aspects and a Model for Calcification. J. Paleontol. 41, 742–762.

747 Treble P.C., Schmitt A.K., Edwards R.L., McKeegan K.D., Harrison T.M., Grove M., Cheng H.
748 and Wang Y.J., 2007. High resolution Secondary Ionisation Mass Spectrometry (SIMS) $\delta^{18}O$
749 analyses of Hulu Cave speleothem at the time of Heinrich Event 1. Chem. Geol. 238, 197–
750 212.

751 Valley J.W. and Kita N.T., 2009. *In situ* oxygen isotope geochemistry by ion microprobe. In
752 MAC Short Course: Secondary Ion Mass Spectrometry in the Earth Sciences (ed. M. Fayek).
753 vol. 41, pp. 16–63.

754 Vetter L., Kozdon R., Mora C.I., Eggins S.M., Valley J.W., Honisch B. and Spero H. J., 2013.
755 Micron-scale intrashell oxygen isotope variation in cultured planktic foraminifers. Geochim.
756 Cosmochim. Ac. 107, 267–278.

757 Vihtakari M., Renaud P.E., Clarke L J., Whitehouse M.J., Hop H., Carroll M.L. and Ambrose
758 W.G. Jr, 2016. Decoding the oxygen isotope signal for seasonal growth patterns in Arctic
759 bivalves. Palaeogeogr. Palaeocl. 446, 263–283.

760 Wacker U., Fiebig J. and Schoene B.R., 2013. Clumped isotope analysis of carbonates:

761 comparison of two different acid digestion techniques. Rapid Commun. Mass Spectrom. 27,
762 1631–1642.

763 Weidel B.C., Ushikubo T., Carpenter S.R., Kita N.T., Cole J.J., Kitchell J.F., Pace M.L. and
764 Valley J.W., 2007. Diary of a bluegill (Lepomis macrochirus): daily $\delta^{13}C$ and $\delta^{18}O$ records in
765 otoliths by ion microprobe. Can. J. Fish. Aquat. Sci. 64, 1641–1645.

766 Wright I.P., 1998. Gas source mass spectrometry. In Encyclopedia of Earth Science Springer
767 Netherlands. pp. 261–262.

768 Wycech J., Kelly D.C. and Marcott S., 2016. Effects of seafloor diagenesis on planktic
769 foraminiferal radiocarbon ages. Geology. 44, 551–554.

770 Wynn P.M., Fairchild I.J., Frisia S., Spötl C., Baker A., Borsato A., EIMF, 2010. High-resolution
771 sulphur isotope analysis of speleothem carbonate by secondary ionisation mass
772 spectrometry. Chem. Geol. 271, 101–107.

773

774 **Table 1** GSMS $\delta^{18}O$ values for UWC-3 calcite. Measurements performed at the University of

775 Wisconsin-Madison previously reported in Kozdon et al. (2009). Accepted value for $\delta^{18}O$

776 (UWC-3) is -17.8 ± 0.1‰ (VPDB) (Kozdon et al., 2009).

Laboratory	Number of Grains per Analysis	Number of Analyses	Sample Weight (µg)	$\delta^{18}O$ (‰, VPDB)		
				Average	2 SD	2 SE
University of Wisconsin-Madison	1-10	9	4,000-8,000	-17.8	0.1	0.1
University of California-Santa Cruz	2-5	3	73-91	-17.9	0.3	0.2
University of California-Davis	1	3	31-40	-17.8	0.2	0.1

777

778 **Table 2** Average SIMS $\delta^{18}O$ values (± 2SE) measured by 3-µm and 10-µm pits in *O. universa*
779 shells collected from the PC9 core-top (untreated) and grown in culture as shown in Figure 3.

Sample	Whole Shell ID	3 µm		10 µm	
		Average $\delta^{18}O$ (‰, VPDB)	n	Average $\delta^{18}O$ (‰, VPDB)	n
PC9 Core-Top (untreated)	A27	-1.5 ± 1.1	4	-0.7 ± 0.3	1
	A35	-1.4 ± 0.6	4	-1.3 ± 0.4	1
	B6	-0.9 ± 0.5	3	-1.7 ± 0.2	2
	B7	-1.3 ± 0.4	9	-1.4 ± 0.4	1
	B9	-1.7 ± 0.5	5	-1.5 ± 0.4	1
	B11	-2.3 ± 0.8	4	-2.1 ± 0.4	1
Culture	CS1	-2.8 ± 0.3	4	-2.6 ± 0.3	1
	CS2	-3.3 ± 0.5	4	-2.4 ± 0.0	2
	CS4	-2.9 ± 0.4	7	-2.2 ± 0.1	3
	CS8	-3.0 ± 0.2	7	-2.4 ± 0.3	2

780 **Table 3** Summary of paired SIMS and GSMS $\delta^{18}O$ measurements of untreated, cleaned, and
781 roasted chambers from PC9 core-top and the cleaned cultured chambers. Number of shells (n)
782 analyzed in each experimental group. Average SIMS and GSMS $\delta^{18}O$ values used to calculate
783 $\Delta^{18}O_{SIMS\text{-}GSMS}$ (±2 SE). The $\Delta^{18}O_{SIMS\text{-}GSMS}$ values of untreated (10-µm pits) and treated shells are
784 significantly different when p-values are less than 0.05. Background-corrected OH/O ratios (± 2
785 SE).

SIMS Spot Size	Sample	Description	n	Average SIMS $\delta^{18}O$ (‰, VPDB)	Average GSMS $\delta^{18}O$ (‰, VPDB)	$\Delta^{18}O_{SIMS\text{-}GSMS}$ (‰)	SIMS vs GSMS $\delta^{18}O$ p-value	$\Delta^{18}O_{SIMS\text{-}GSMS}$ Untreated-Treated p-value	Average $^{16}OH/^{16}O$
3-µm	PC9 (0-3 cm)	Untreated	15	-1.7 ± 0.4	-0.7 ± 0.4	-1.0 ± 0.2	3.7×10^{-8} *	0.14	$(12.1 \pm 3.1) \times 10^{-3}$
10-µm	PC9 (0-3 cm)	Untreated	11	-1.6 ± 0.3	-0.8 ± 0.2	-0.8 ± 0.2	3.3×10^{-5} *	NA	$(9.4 \pm 0.6) \times 10^{-3}$
	PC9 (0-3 cm)	Hydrogen Peroxide Cleaned, Sonicated	15	-1.7 ± 0.2	-0.8 ± 0.2	-0.9 ± 0.1	7.2×10^{-10} *	0.52	$(9.6 \pm 0.3) \times 10^{-3}$
	PC9 (0-3 cm)	Roasted	13	-1.3 ± 0.5	-0.6 ± 0.4	-0.7 ± 0.2	1.2×10^{-5} *	0.82	$(1.4 \pm 0.4) \times 10^{-3}$
	Culture	Hydrogen Peroxide Cleaned	8	-2.4 ± 0.1	-1.7 ± 0.2	-0.7 ± 0.1	4.8×10^{-6} *	0.72	$(8.7 \pm 0.8) \times 10^{-3}$

*Difference is statistically significant

Table 4 Minor element composition of the UWC-3 standard and *O. universa* calcite. Element composition of UWC-3 previously reported in Kozdon et al. (2009). *O. universa* shells analyzed in previous studies were either grown in laboratory culture or recovered from pelagic sediments.

Element	Concentration (ppmw)		*O. universa* References
	UWC-3	*O. universa*	
Mg	5,457	243-4,127	Boyle, 1981; Carpenter and Lohmann, 1992; Delaney et al., 1985; Eggins et al., 2004; Lea et al., 1999; Russell et al., 2004; Sadekov et al., 2005; Spero et al., 2015
Fe	4,046	95-323	Boyle, 1981
Sr	2,227	1,050-1,576	Carpenter and Lohmann, 1992; Delaney et al., 1985; Lea et al., 1999; Russell et al., 2004; Bender et al., 1975
Mn	1,222	37-40	Boyle, 1981
Ba	1,234	1.1-5.5	Lea et al., 1999; Lea and Boyle, 1991

Figure 1 Scanning electron microscope (SEM) images depicting chamber fragmentation method used in this study. All scale bars are 100 μm. A. Back-scattered electron (BSE) SEM image of intact *O. universa* shell taken from the core-top of PC9. B. BSE SEM image of the final chamber fragment used for GSMS analysis. C. Secondary electron (SE) SEM image of remaining fragment cast in epoxy and cross-sectioned for SIMS analysis.

Figure 2 SEM images showing final chamber fragments of *O. universa* in cross-section with transects of 3-μm SIMS analysis pits and their corresponding $\delta^{18}O$ values (error bars: horizontal = width of SIMS pits, vertical = analytical precision, 2 SD). All chamber fragments shown are from PC9 core-top specimens, arrows point toward chamber wall exterior, and dashed lines extending across plotted $\delta^{18}O$ data denote mean value for each chamber fragment. Results are representative of 3-μm and 10-μm SIMS spot analyses. A. Cross-section of chamber fragment cast in epoxy (black) with original whole shell in inset (scale bars = 100 μm). Box overlain on chamber cross-section delimits area of SIMS transect shown in B. B. Transect of SIMS pits

803 across cross-section of chamber wall shown in A (scale bar = 5 μm). C. $\delta^{18}O$ values for SIMS
804 pits shown in B plotted against distance from chamber wall interior. D-F. Upper panels showing
805 transects of SIMS analysis pits running across cross-sections of chamber walls (scale bars = 5
806 μm), lower panels show corresponding $\delta^{18}O$ values plotted against distance from chamber wall
807 interior.

808 **Figure 3** Comparison of intra-chamber $\delta^{18}O$ values measured with 3-μm and 10-μm SIMS
809 analysis pits in *O. universa* chambers. A. Untreated chamber fragments of shells from PC9 core-
810 top, B. cleaned chamber fragments of cultured shells. Labels along abscissa are the whole shell
811 ID numbers (see Appendix B). Individual analyses (small symbols) are from 3-μm pits (open
812 symbols) and 10-μm pits (filled symbols) with average $\delta^{18}O$ values per shell (large symbols).
813 Error bars are external precision on individual SIMS $\delta^{18}O$ values (± 2 SD).

814 **Figure 4** Comparison of paired SIMS and GSMS $\delta^{18}O$ values from the same chamber of *O.*
815 *universa* shells. Theoretical 1-to-1 lines (solid bold lines) denote no difference between
816 corresponding SIMS and GSMS $\delta^{18}O$ values. Linear regression with slope=1 (dashed lines) fit to
817 data. A. Untreated core-top shells (3-μm SIMS analyses), B. untreated core-top shells (10-μm
818 SIMS analyses), C. cleaned core-top shells (10-μm SIMS analyses), D. roasted core-top shells
819 (10-μm SIMS analyses), and E. cleaned shells from culture experiment (10-μm SIMS analyses).
820 All SIMS data shown are average chamber values. Error bars are GSMS analytical precision (±2
821 SD, horizontal) and propagated error from multiple SIMS measurements per shell (±2 SE,
822 vertical). F. Histogram of $\Delta^{18}O_{SIMS\text{-}GSMS}$ values for the paired datasets in A-E. Average $\Delta^{18}O_{SIMS\text{-}GSMS}$ value (dashed vertical line).

824 **Figure 5** Comparison of GSMS $\delta^{18}O$ values measured from unroasted and roasted fragments of
825 the same *O. universa* shell. Robust regression using iteratively reweighted least squares (dashed
826 line) with corresponding slope (m) and y-intercept (b). 95% confidence interval on the slope
827 (0.89 to 0.99) and y-intercept (-0.2 to -0.1) (grey shading). R^2 from unweighted least squares
828 regression. Theoretical 1-to-1 line denoting no difference (solid line). Error bars express external
829 instrumental precision (±2 SD).

830 **Figure 6** Adjusted (+0.9‰) SIMS $\delta^{18}O$ values plotted against GSMS $\delta^{18}O$ values from the same
831 chamber of *O. universa* shells. Theoretical 1-to-1 line (solid bold line) denotes no SIMS-GSMS
832 $\delta^{18}O$ difference. Linear regression with slope=1 (dashed lines) fit to data. A. Untreated core-top
833 shells (3-µm SIMS analyses), B. untreated core-top shells (10-µm SIMS analyses), C. cleaned
834 core-top shells (10-µm SIMS analyses), D. roasted core-top shells (10-µm SIMS analyses), and
835 E. cleaned shells from culture experiment (10-µm SIMS analyses). All SIMS data shown are
836 average chamber values, and have been adjusted (see Section 3.2). Error bars are GSMS
837 analytical precision (±2 SD, horizontal) and propagated error from SIMS measurements (±2 SD,
838 vertical). F. Histogram of adjusted $\Delta^{18}O_{SIMS\text{-}GSMS}$ values for the paired datasets in A-E. Average
839 adjusted $\Delta^{18}O_{SIMS\text{-}GSMS}$ value (dashed vertical line).

840 **Figure 7** Average $\Delta^{18}O_{SIMS\text{-}GSMS}$ values plotted against background-corrected OH/O ratios
841 measured for *O. universa* chambers that were untreated (circles), cleaned with hydrogen
842 peroxide and sonication (diamond), and roasted (square) from the Site PC9 core-top (CT), and
843 for cultured (Cult) *O. universa* chambers cleaned with hydrogen peroxide (triangle). Note:
844 $\Delta^{18}O_{SIMS\text{-}GSMS}$ for untreated chambers measured using 10-µm (large circle) and 3-µm (small

845 circle) SIMS pits. Error bars are 2 times the standard error of the OH/O ratio mean (horizontal)

846 and the $\Delta^{18}O_{SIMS\text{-}GSMS}$ mean (vertical).

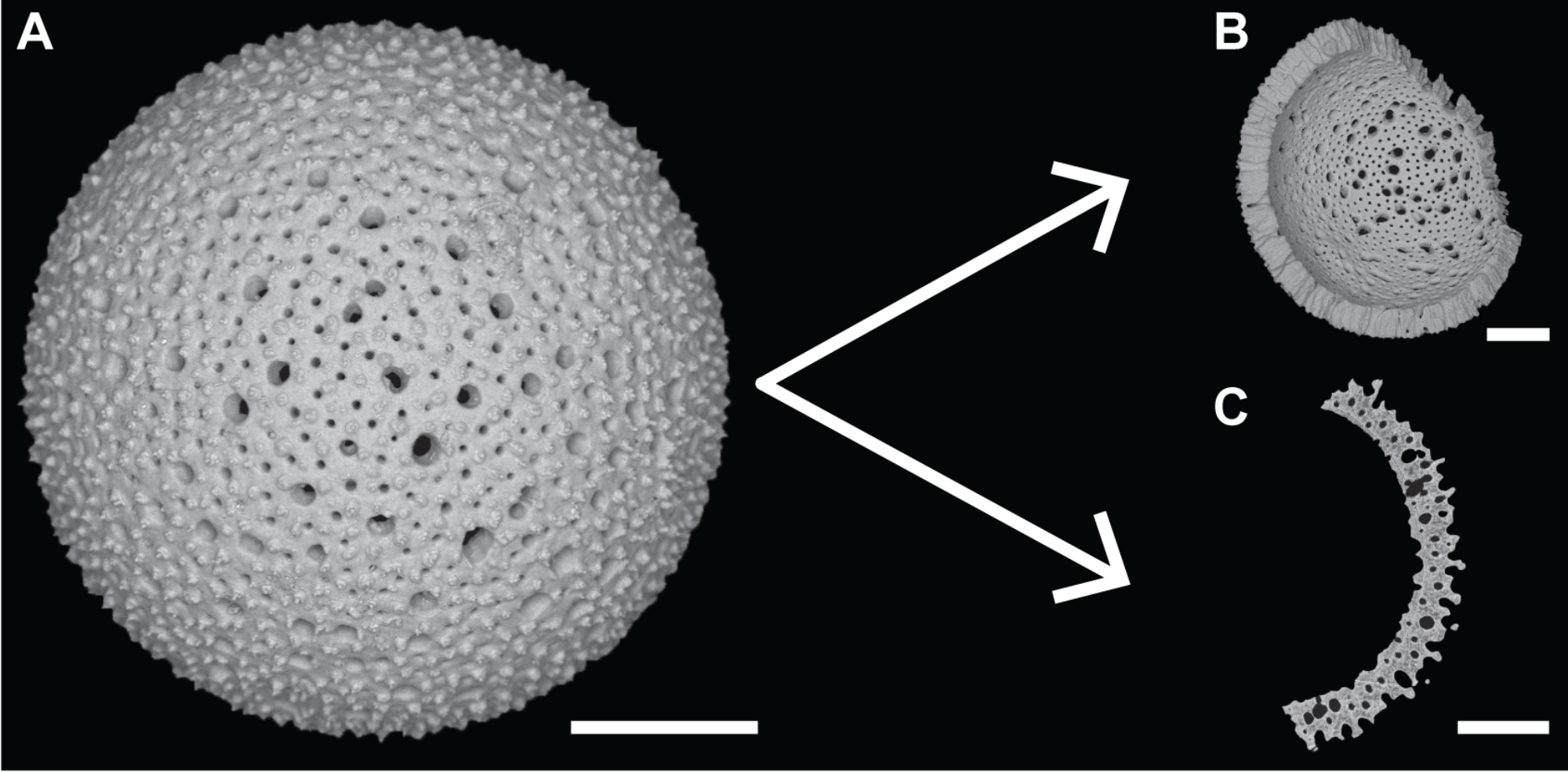

Figure 1

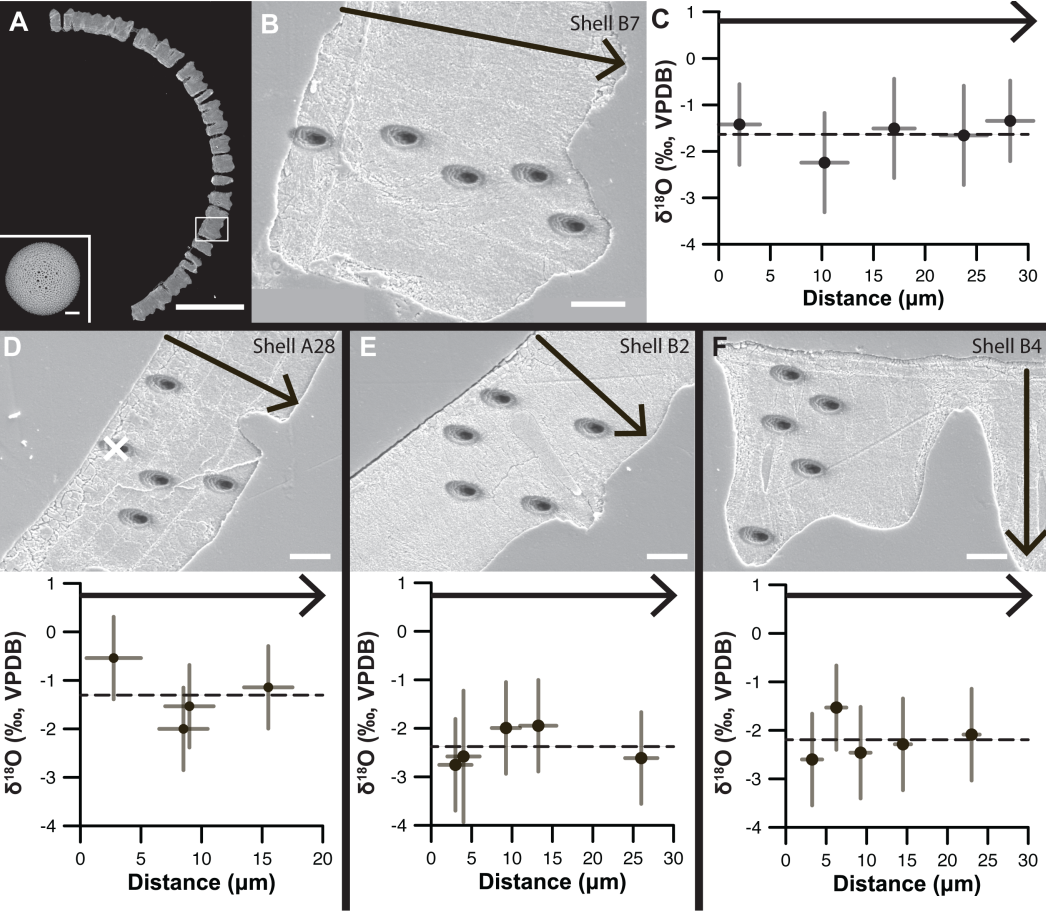
A
B
Shell B7
C
δ18O (‰, VPDB)
Distance (μm)
D
Shell A28
E
Shell B2
F
Shell B4

Figure 2

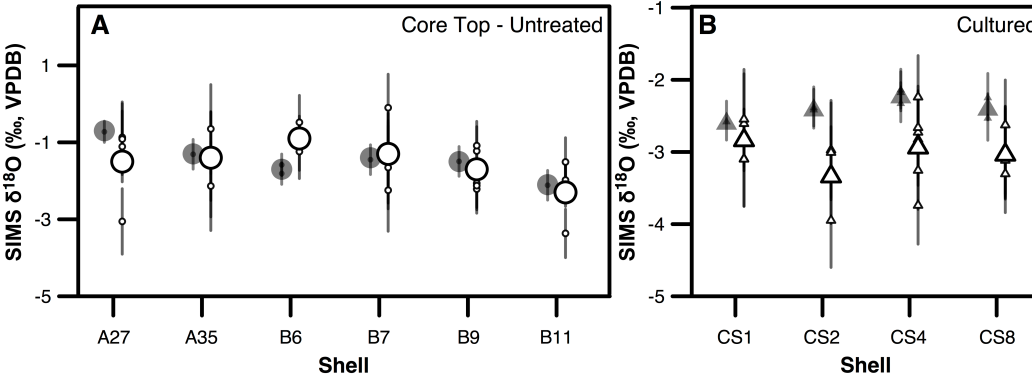
A
Core Top - Untreated
SIMS δ18O (‰, VPDB)
1
-1
-3
-5
A27
A35
B6
B7
B9
B11
Shell
B
Cultured
-1
-2
-3
-4
-5
CS1
CS2
CS4
CS8
Shell

Figure 3

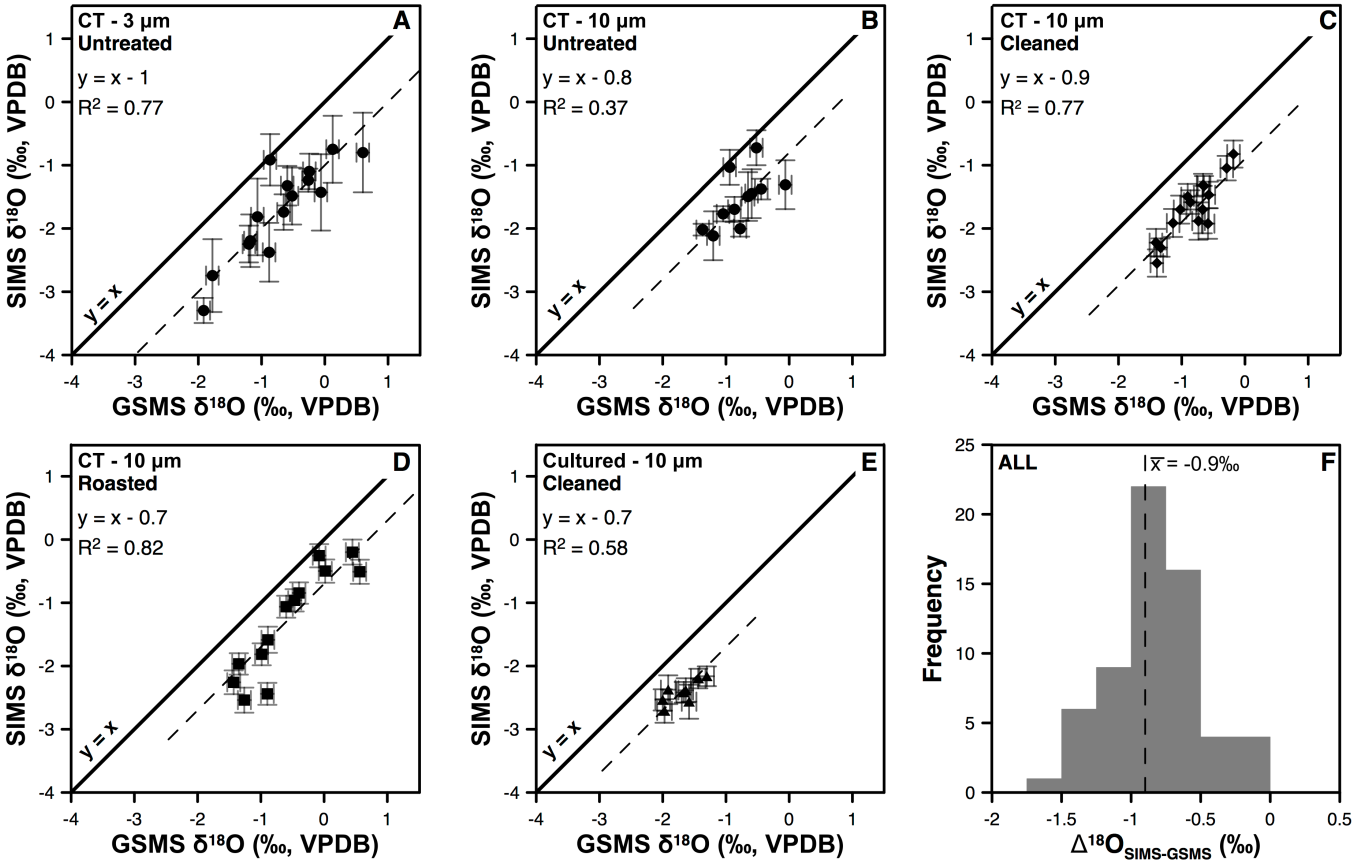
CT - 3 µm
Untreated
A
y = x - 1
R² = 0.77
y = x
SIMS δ18O (‰, VPDB)
GSMS δ18O (‰, VPDB)
CT - 10 µm
Untreated
B
y = x - 0.8
R² = 0.37
y = x
SIMS δ18O (‰, VPDB)
GSMS δ18O (‰, VPDB)
CT - 10 µm
Cleaned
C
y = x - 0.9
R² = 0.77
y = x
SIMS δ18O (‰, VPDB)
GSMS δ18O (‰, VPDB)
CT - 10 µm
Roasted
D
y = x - 0.7
R² = 0.82
y = x
SIMS δ18O (‰, VPDB)
GSMS δ18O (‰, VPDB)
Cultured - 10 µm
Cleaned
E
y = x - 0.7
R² = 0.58
y = x
SIMS δ18O (‰, VPDB)
GSMS δ18O (‰, VPDB)
ALL
x̄ = -0.9‰
F
Frequency
Δ18OSIMS-GSMS (‰)

Figure 4

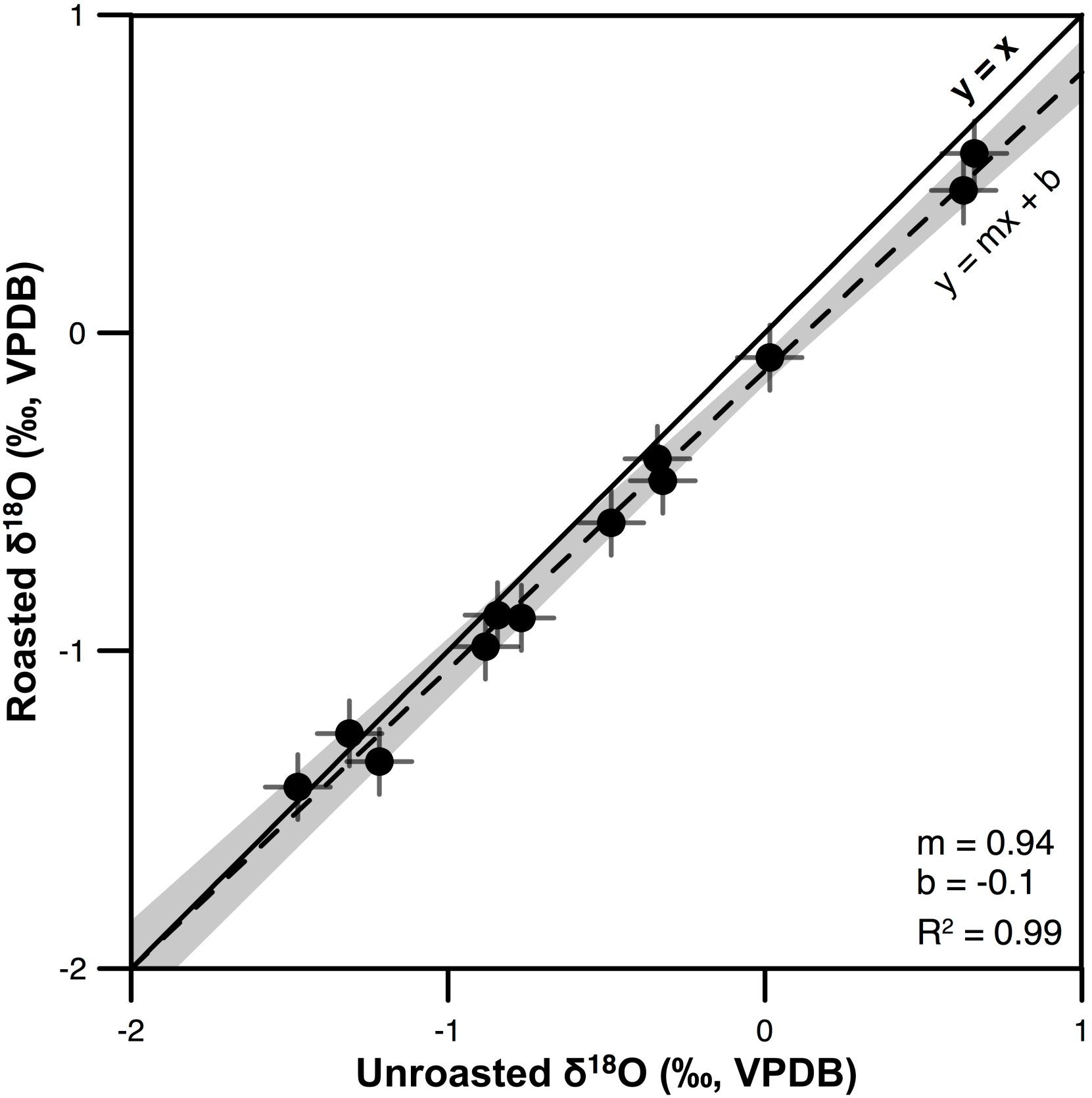
y = x
y = mx + b
m = 0.94
b = -0.1
R² = 0.99
Roasted δ18O (‰, VPDB)
Unroasted δ18O (‰, VPDB)
1
0
-1
-2
-2
-1
0
1

Figure 5

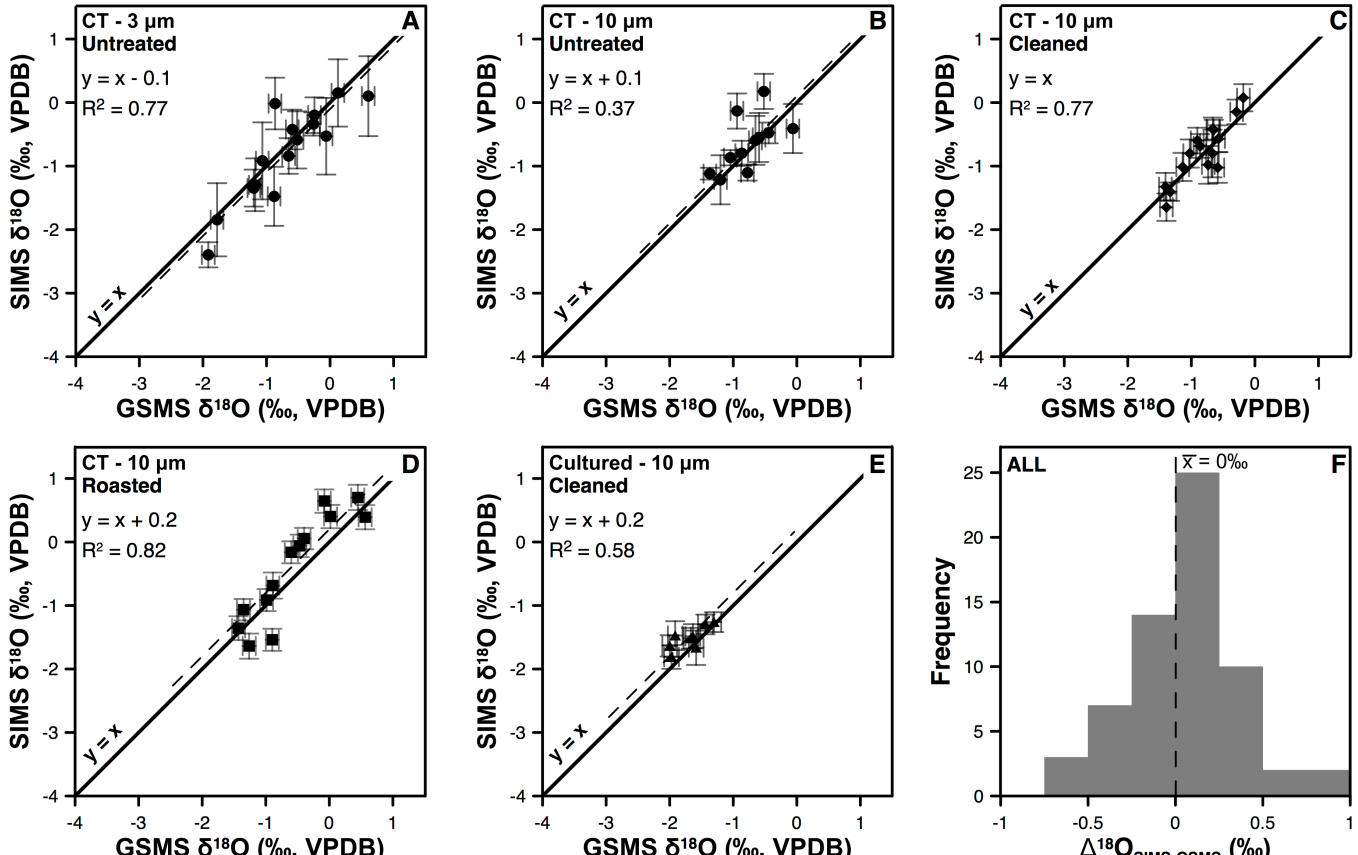
CT - 3 µm
Untreated
A
y = x - 0.1
R² = 0.77
y = x
SIMS δ18O (‰, VPDB)
GSMS δ18O (‰, VPDB)
CT - 10 µm
Untreated
B
y = x + 0.1
R² = 0.37
y = x
SIMS δ18O (‰, VPDB)
GSMS δ18O (‰, VPDB)
CT - 10 µm
Cleaned
C
y = x
R² = 0.77
y = x
SIMS δ18O (‰, VPDB)
GSMS δ18O (‰, VPDB)
CT - 10 µm
Roasted
D
y = x + 0.2
R² = 0.82
y = x
SIMS δ18O (‰, VPDB)
GSMS δ18O (‰, VPDB)
Cultured - 10 µm
Cleaned
E
y = x + 0.2
R² = 0.58
y = x
SIMS δ18O (‰, VPDB)
GSMS δ18O (‰, VPDB)
ALL
F
x̄ = 0‰
Frequency
Δ18OSIMS-GSMS (‰)

Figure 6

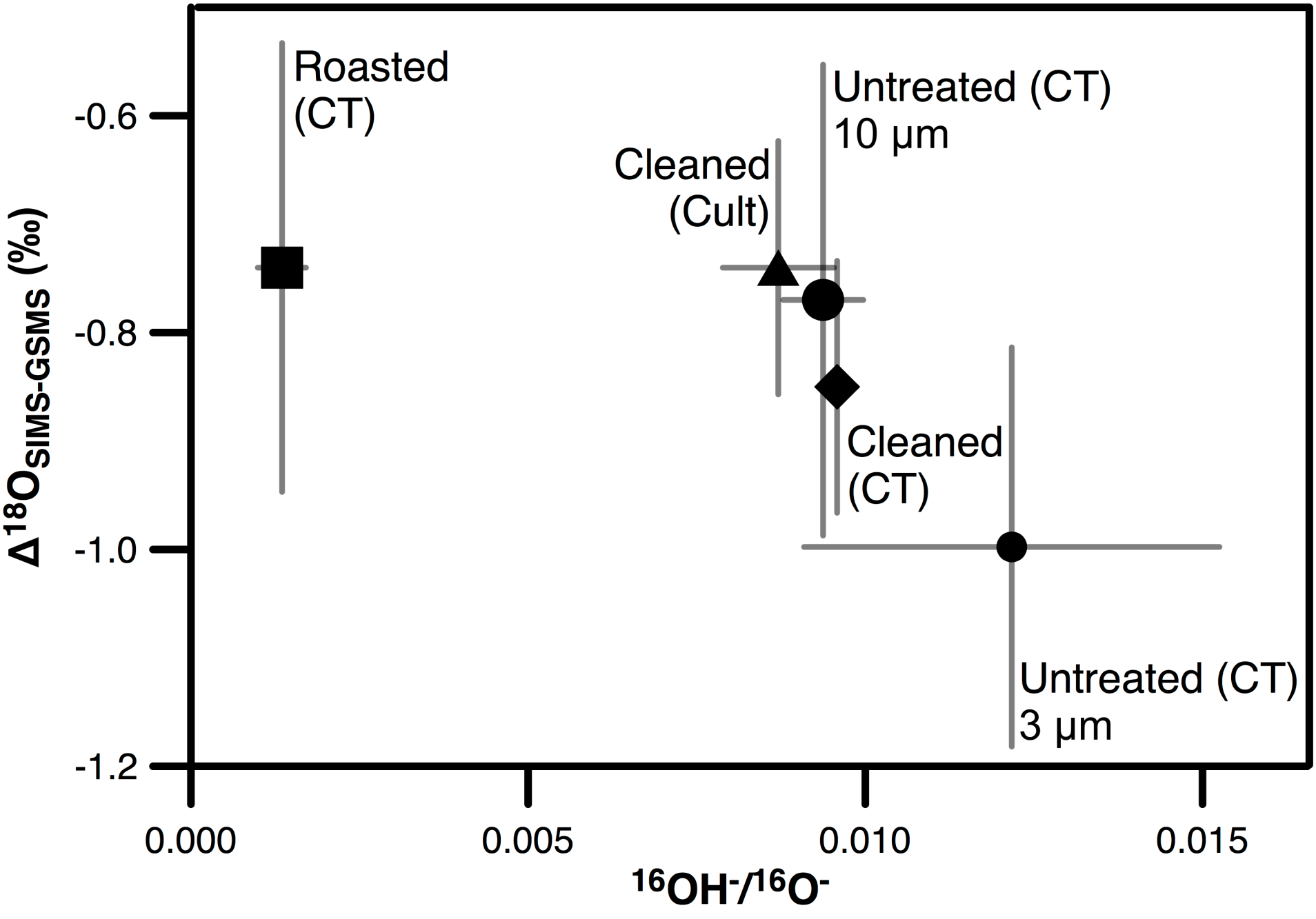
Roasted
(CT)
Cleaned
(Cult)
Untreated (CT)
10 µm
Cleaned
(CT)
Untreated (CT)
3 µm
-0.6
-0.8
-1.0
-1.2
0.000
0.005
0.010
0.015
Δ18OSIMS-GSMS (‰)
16OH-/16O-

Figure 7

Appendix A. Supplementary Material

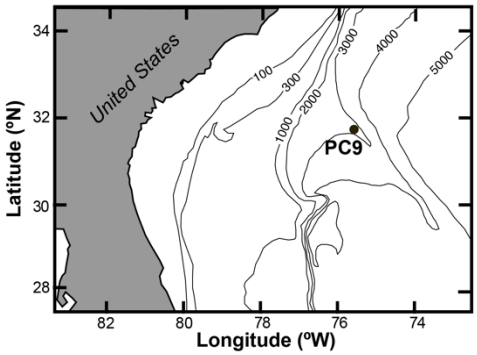

Figure S1 Map showing location and bathymetric setting of study area from which piston core PC9 was retrieved (contour lines in meters).

S1. SIMS $\delta^{18}O$ Data Processing

The quality of each SIMS $\delta^{18}O$ analysis was evaluated on the basis of pit appearance by SEM (Fig. S1) and secondary ion yield ($^{16}O^-$) relative to that of the bracketing standard analyses. The primary beam current was not recorded during 3-μm SIMS sessions, so the $^{16}O^-$ count rate shell/standard ratio instead of the secondary ion yield ($^{16}O^-$) was used to assess the resulting data from these sessions. Acceptable shell/standard ratio "cut-offs" were assessed by session-specific examination of the covariance of $\delta^{18}O$ with the ratios. The cutoff for each session was defined based on the Tukey-outlier method (Tukey, 1977), and typically indicated that shell yield or $^{16}O^-$ count rate ratios below 92-95% of the standard had statistically lower $\delta^{18}O$ values. The pit appearance and paired $\delta^{18}O$ value were each assigned a score from 1 to 3 (good=1, questionable=2, irregular=3) using a method that was blind to the other metric, i.e. pit appearance was scored without knowing the paired $\delta^{18}O$ value and vice versa. Pits were given a score of 3 if it crosscut cracks or had irregular internal structure (Fig. S1D). The latter suggests that the pit intersected porous domains, inclusions, or voids. The scores determined from pit appearance were used to assign a final score to the analysis using the same scale from 1 to 3. In

cases where both pit appearance and data quality were scored as 1, the analysis was assigned a final score of 1. Similarly, in cases where both pit appearance and data quality were questionable (score=2), the analysis was assigned a final score of 2. If either the pit appearance or data quality were irregular (score=3), the analysis was assigned a final score of 3. Several analyses had pit appearance and data quality scores that were either good or questionable (scored ≤ 2), but were not in agreement with one another (i.e. the pit looked good while the ion yield ratios were questionable and vice versa). For these analyses, the $\delta^{18}O$ values were evaluated relative to other measurements taken from the same shell. If the measured $\delta^{18}O$ value for the investigated datum was within the external analytical precision (±2 SD) of the other SIMS measurements from the same shell, the point was given a final score of 1. However, if the measured $\delta^{18}O$ value for the investigated datum exceeded the external analytical precision of the other measurements from the same shell or if the analysis was the only measurement from that shell, the datum was deemed questionable (final score=2). Only data with a final score of 1 are plotted and discussed in the manuscript.

Although OH/O ratios negatively correlate with the measured $\delta^{18}O$ value, the ratios were not used for quality control purposes because $^{16}O^-$ ion yield and count rate were more sensitive to the quality of the data. The background-corrected OH/O ratios varied between 0.0002-0.06 within the *O. universa* chambers measured in this study, and still provide useful insight into the relative amount of hydrogen-bearing phases (i.e. water or organics) within the foraminifer calcite.

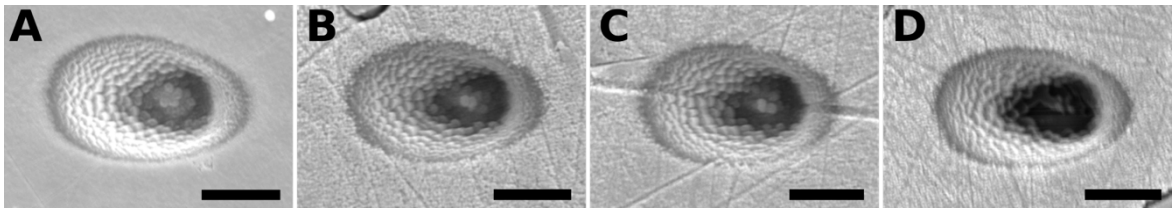

Figure S2 Scanning electron microscope SE images of 10-µm SIMS $\delta^{18}O$ analysis pits for A. UWC-3 calcite standard, and foraminifer shell analysis pits with a ranking of B. 1 (good), C. 2 (questionable), and D. 3 (irregular). Note the cross-cutting crack in C and the misshapen pit bottom in D. All scale bars are 5 µm.

S2. Effect of sample treatment on SIMS and GSMS $\delta^{18}O$ values

The effect of sample treatment on $\delta^{18}O$ measurements is investigated by separate comparison of the SIMS and GSMS values from in each experiment (Figs. S2, S3).

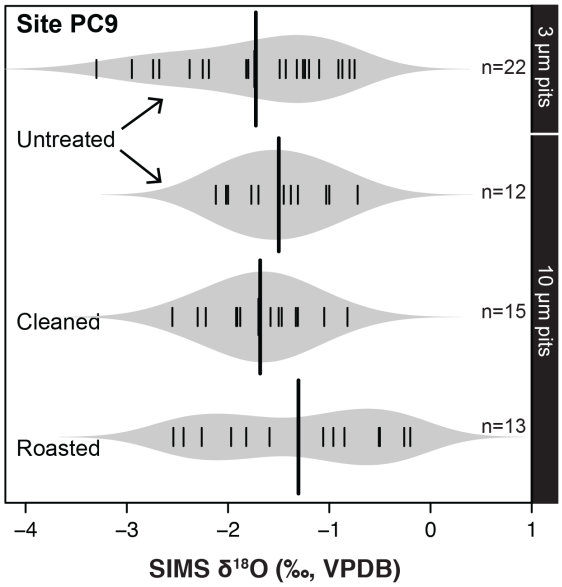

Figure S3 Spindle diagrams of SIMS $\delta^{18}O$ values of the untreated, cleaned (hydrogen peroxide, sonicated), and roasted *O. universa* fragments from the Site PC9 core top measured with 3-µm and 10-µm pits. Grey spindles are kernel bean distribution of mean $\delta^{18}O$ values per shell (small vertical lines). Average $\delta^{18}O$ values per experiment (bold vertical lines). Number of shells (n) analyzed per experiment.

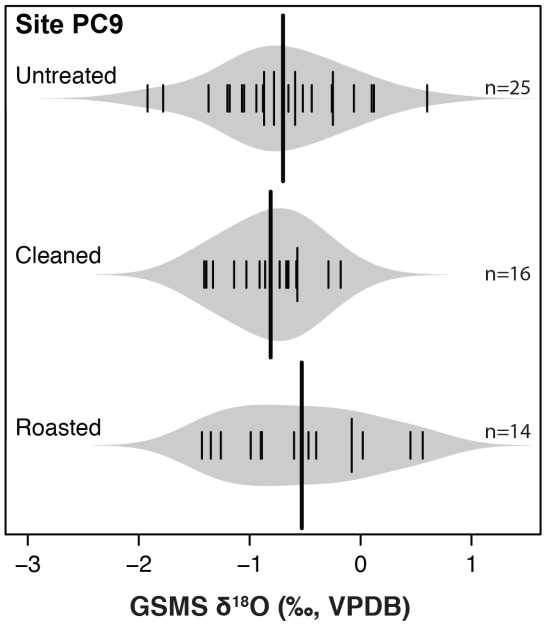

Figure S4 Spindle diagrams of GSMS $\delta^{18}O$ values of the untreated, cleaned (hydrogen peroxide, sonicated), and roasted *O. universa* fragments from the Site PC9 core top. Grey spindles are kernel bean distribution of individual chamber $\delta^{18}O$ values (small vertical lines). Some shells have the same $\delta^{18}O$ values (taller thin vertical lines). Mean $\delta^{18}O$ values per experiment (bold vertical lines). Number of shells (n) analyzed per experiment.

S3. Comparison of surface structures and $\Delta^{18}O_{SIMS\text{-}GSMS}$ values

In seafloor sediments, variability in shell appearance can reflect differences in preservation. Translucent (glassy) shells are considered relatively pristine and unaffected by post-depositional chemical reactions with sedimentary pore fluids, whereas opaque (frosty) shells exhibit a milky white hue under reflected light presumably due to the presence of an external coating of secondary carbonate added to the shell surface via early diagenesis (e.g., Pearson et al., 2001; Sexton et al., 2006; Pearson et al., 2007; Wycech, Kelly and Marcott, 2016). In addition, partial dissolution has also been shown to affect foraminifer shell textures and morphological features (Bé et al., 1975; Hecht et al., 1975; Regenberg and Beil, 2016). Alternatively, such differences in optical appearance or surface textures of *O. universa* shells may reflect genotypic variation in shell wall thickness and textures (e.g., De Vargas et al., 1999; Morard et al., 2009), and/or differing reproductive histories.

Prior to fragmentation, whole shell images of the untreated and cleaned specimens analyzed were taken using back-scattered electron (BSE) imaging on a Hitachi S-3400N scanning electron microscope (SEM) in variable pressure mode (Appendix B). The varying $\Delta^{18}O_{SIMS\text{-}GSMS}$ values registered by *O. universa* chambers with differing surface textures and optical appearances (Fig. S5F-G) suggest that the SIMS-GSMS differences are not related to inter-shell differences in preservation, gametogenesis, or genotype. This is best exemplified by the measured SIMS-GSMS $\delta^{18}O$ differences amongst the translucent shells, which contradicts the supposition that the inter-instrumental $\delta^{18}O$ difference was caused by GSMS measurement of a thin diagenetic veneer on the opaque shells. We caution, however, that this finding does not preclude the possibility that some of the variation in shell appearance is caused by early diagenesis at PC9. This is especially true if the secondary carbonate is added through mineral replacement, not as a

thin veneer on the exterior of the shell.

The presence of frosty foraminifers in the Site PC9 sample suggest that diagenetic alteration of the core top shells is possible but most likely not a major contributor to the SIMS-GSMS $\delta^{18}O$ difference. Moreover, the analyzed *O. universa* chambers grown in culture were never exposed to water column or seafloor conditions, yet paired SIMS-GSMS $\delta^{18}O$ values differ by 0.7‰. This result provides the strongest argument against a diagenetic or dissolution mechanism for the inter-instrumental $\delta^{18}O$ difference.

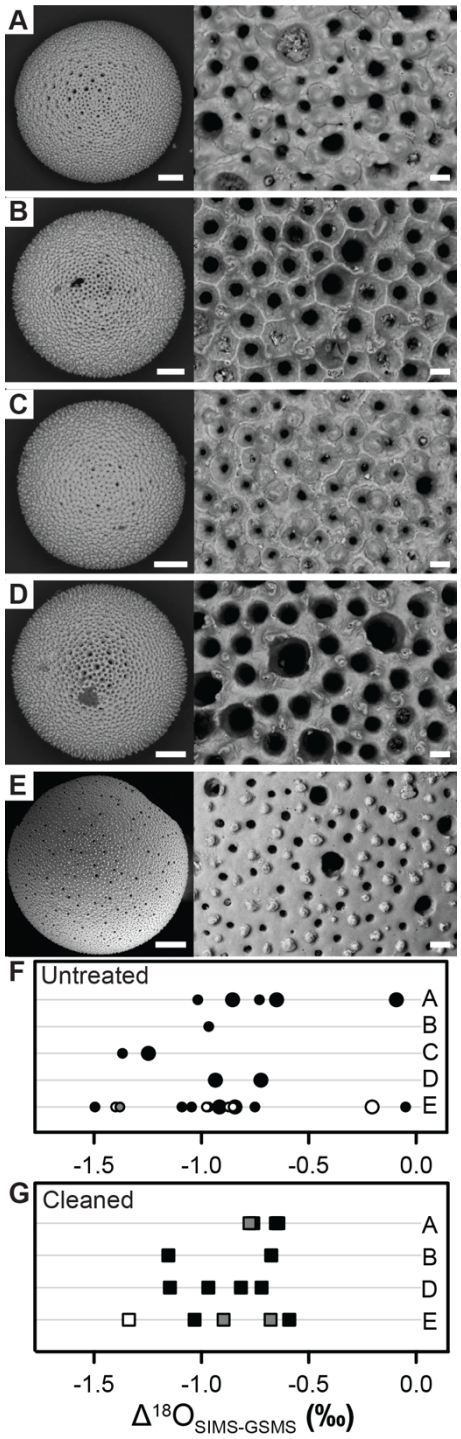

Figure S5. Comparison of surface textures of *O. universa* shells from the PC9 core top to their corresponding SIMS-GSMS $\delta^{18}O$ offsets. A-E. Scanning electron BSE images of shells (left, scale bars = 100 μm) and highly magnified images of surface textures (right, scale bars = 10 μm) for five different *O. universa* morphotypes. Shell textures are distinguished as A. variable pore sizes with calcite mounds at spine bases, B. large pores of uniform size, cancellate texture with pointed/etched spine bases, C. small pores of uniform size with inter-pore ridges, calcite mounds at spine bases, D. variable pore sizes, steeply-sloped pore walls, terraced spine bases, E. smooth surface with varying pore sizes and broken spines possessing terraced bases. Under optical light, morphotypes A-D are opaque, morphotype E includes shells with opaque, translucent, or intermediate appearances. F. $\Delta^{18}O_{SIMS\text{-}GSMS}$ values for untreated *O. universa* shells separated by shell textures (A-E) and optical appearance. $\Delta^{18}O_{SIMS\text{-}GSMS}$ values are from 3-μm (small circles) and 10-μm (large circles) SIMS pits. G. $\Delta^{18}O_{SIMS\text{-}GSMS}$ values for cleaned *O. universa* shells separated by shell textures (A-E) and optical appearance. $\Delta^{18}O_{SIMS\text{-}GSMS}$ values are difference between 10-μm SIMS and GSMS $\delta^{18}O$ values. F-G. Note that, under reflected light, "opaque" shells (black filled symbols) appear white, "translucent" shells (open symbols) are glassy, and intermediate shells (grey filled symbols) have an appearance between translucent and opaque.

Table S1 Sample numbers of cultured *O. universa* specimens used in this study. Specimens were grown at constant temperature (22 ± 0.2°C), $\delta^{18}O_{sw}$ = -0.25 ± 0.05‰ (VSMOW), salinity = 33.3‰, pH =8.04, and with an ambient [CO_3^{2-}] (2250 μmol kg^{-1}). Measured SIMS $\delta^{18}O$ values are provided in Table S2. Measured GSMS $\delta^{18}O$ values are provided in Tables S3 and S4.

Light Cycle	ID (Spero Lab)	Whole Shell ID (this study)
12 hour:12 hour low light:dark	CH303, CH302	CS1, CS2
24 hour low light	CH60, CH61, CH62	CS4, CS5, CS6
12 hour:12 hour high light:dark	CH114, CH122, CH124	CS7, CS8, CS9

Table S2: Unadjusted 10-μm and 3-μm SIMS $\delta^{18}O$ measurements of *O. universa* chamber fragments of shells grown in culture and recovered from the PC9 core top.

Table S3: Paired GSMS and 10-μm SIMS pit $\delta^{18}O$ values measured from *O. universa* fragments of shells grown in culture and collected from the Site PC9 core top.

Table S4: Paired GSMS and 3-μm SIMS pit $\delta^{18}O$ values measured from *O. universa* fragments of shells grown in culture and collected from the Site PC9 core top.

Table S5 Summary of unpaired $\delta^{18}O$ values measured by GSMS and SIMS (± 2 SE). Number of shells analyzed (n) is larger than that noted in Table 2 because not all shells analyzed have paired SIMS-GSMS $\delta^{18}O$ values. P-values provided by unpaired t-test on mean $\delta^{18}O$ per shell datasets of the treated and untreated experiments. $\Delta^{18}O_{Treated-Untreated}$ values are not statistically significant given that all p-values are greater than 0.05.

Analytical Technique	Treatment	n	Average $\delta^{18}O$ (‰, VPDB)	$\Delta^{18}O_{Treated-Untreated}$	p-value
SIMS (3-µm pits)	Untreated	22	-1.7 ± 0.3	NA	NA
SIMS (10-µm pits)	Untreated	12	-1.5 ± 0.3	NA	NA
	Cleaned	15	-1.7 ± 0.2	-0.2	0.307
	Roasted	13	-1.3 ± 0.5	0.2	0.474
GSMS	Untreated	25	-0.7 ± 0.2	NA	NA
	Cleaned	16	-0.8 ± 0.2	-0.1	0.458
	Roasted	14	-0.5 ± 0.3	0.2	0.423

Table S6 Slope, y-intercept, and 95% confidence interval (CI) provided by robust regression analysis of GSMS $\delta^{18}O$ values versus unadjusted and adjusted SIMS $\delta^{18}O$ values for all experiments. The SIMS vs GSMS $\delta^{18}O$ relationship is shown by fitting linear regressions with slope=1 to data (see Figs. 4, 6).

SIMS Spot Size	Sample	Description	slope	95% CI	Unadjusted		Adjusted	
					y-intercept	95% CI	y-intercept	95% CI
3-µm	PC9 (0-3 cm)	Untreated	1.0	0.7 to 1.2	-1.0	-1.3 to -0.8	-0.1	-0.4 to 0.1
10-µm	PC9 (0-3 cm)	Untreated	0.7	0.5 to 0.9	-1.0	-1.3 to -0.9	-0.2	-0.4 to 0
	PC9 (0-3 cm)	Hydrogen Peroxide Cleaned, Sonicated	1.1	0.8 to 1.4	-0.7	-1.0 to -0.4	0.2	-0.1 to 0.5
	PC9 (0-3 cm)	Roasted	1.2	0.8 to 1.5	-0.6	-0.9 to -0.3	0.3	0 to 0.6
	Culture	Hydrogen Peroxide Cleaned	0.6	0.1 to 1.1	-1.4	-2.3 to -0.5	-0.5	-1.4 to 0.4

Table S7 GSMS $\delta^{18}O$ values for roasted and unroasted fragments of the same *O. universa* shell (>355 μm size fraction). Analytical precision is 0.10‰ (2SD).

Whole Shell ID	Roasted		Unroasted	
	Fragment Weight (μg)	$\delta^{18}O$ (‰, VPDB)	Fragment Weight (μg)	$\delta^{18}O$ (‰, VPDB)
S1	26	-0.89	47	-0.84
S2	26	-0.40	18	-0.34
S4	43	-1.35	22	-1.22
S5	21	-1.43	31	-1.47
S6	94	0.45	57	0.63
S7	30	-1.26	47	-1.31
S8	27	0.56	29	0.66
S9	58	-0.99	40	-0.88
S10	28	-0.90	25	-0.77
S11	49	-0.08	62	0.01
S12	39	-0.60	21	-0.49
S13	42	-0.47	23	-0.32

References

Bé, A.W., Morse, J.W., Harrison, S.M., Progressive dissolution and ultrastructural breakdown in planktonic foraminifera, *Special Publications - Cushman Foundation for Foraminiferal Research* **13**, 1975, 27–55.

De Vargas, C., Norris, R.D., Zaninetti, L., Gibb, S.W., Pawlowshi, J., Molecular evidence of cryptic speciation in planktonic foraminifers and their relation to oceanic provinces. *P. Natl. Acad. Sci.* **96**, 1999, 2864–2868.

Hecht, A.D., Eslinger, E.V., Garmon, L.B., Experimental studies on the dissolution of planktonic foraminifera, in: Sliter, W.V., Be, A.W.H., Berger, W.H. (Eds.), Dissolution of Benthic Carbonates, *Special Publications - Cushman Foundation for Foraminiferal Research*, 1975, pp. 56–69.

Morard, R., Quillévéré, F., Escarguel, G., Ujiie, Y., de Garidel-Thoron, T., Norris, R.D., De Vargas, C., Morphological recognition of cryptic species in the planktonic foraminifer *Orbulina universa*. *Mar. Micropaleontol.* **71**, 2009, 148–165.

Pearson, P.N., Ditcheld, P.W., Singano, J., Harcourt-Brown, K.G., Nicholas, C.J., Shackleton, N.J., Hall, M.A., Warm tropical sea surface temperatures in the Late Cretaceous and Eocene epochs, *Nature* **415**, 2001, 481–487.

Pearson, P.N., Van Dongen, B.E., Nicholas, C.J., Pancost, R.D., Schouten, S., Singano, J.M., Wade, B.S., Stable warm tropical climate through the Eocene Epoch, *Geology* **35**, 2007, 211–214.

Regenberg, M., Beil, S., Test appearance of the planktonic foraminifer *Pulleniatina obliquiloculata* as an indicator of calcite dissolution in deep-sea sediments, *J. Foramin. Res.* **46**, 2016, 224–236.

Sexton, P.F., Wilson, P.A., Pearson, P.N., Microstructural and geochemical perspectives on planktic foraminiferal preservation: "Glassy" versus 'Frosty', *Geochem. Geophy. Geosy.* **7**, 2006, 1–29.

Tukey J. W., Exploratory Data Analysis. In *The Future of Data Analysis* Addison-Wesley Publishing Co., Reading, 1977.

Wycech, J., Kelly, D.C., Marcott, S., Effects of seafloor diagenesis on planktic foraminiferal radiocarbon ages, *Geology* **44**, 2016, 551–554.